ACS OMEGA

http://pubs.acs.org/journal/acsodf

Article

Study on Typical Diarylurea Drugs or Derivatives in Cocrystallizing with Strong H-Bond Acceptor DMSO

Chengwei Li,[‖] Jialiang Zhong,[‖] Baohu Liu, Tao Yang, Binhua Lv,* and Youfu Luo*

Cite This: *ACS Omega* 2021, 6, 5532−5547

Read Online

ACCESS | Metrics & More | Article Recommendations | Supporting Information

ABSTRACT: Diarylureas are widely used in self-assembly and supramolecular chemistry owing to their outstanding characteristics as both H-bond donors and acceptors. Unfortunately, this bonding property is rarely applied in the development of urea-containing drugs. Herein, seven related dimethyl sulfoxide (DMSO) complexes were screened from 12 substrates involving sorafenib and regorafenib, mainly considering the substitution effect following a robust procedure. All complexes were structurally confirmed by spectroscopic means and thermal analysis. Specially, five cocrystals with three deuterated, named sorafenib·DMSO, donafenib·DMSO, deuregorafenib·DMSO, **6**·DMSO, and **7**·DMSO were obtained. The crystal structures revealed that all host molecules consistently bonded with DMSO in intermolecular interaction in a 1:1 stoichiometry. However, further comparison with documented DMSO complexes and parent motifs presented some arrangement diversities especially for **6**·DMSO which offered a counter-example to previous rules. Major changes in the orientation of meta-substituents and the packing stability for sorafenib·DMSO and deuregorafenib·DMSO were rationalized by theory analysis and computational energy calculation. Cumulative data implied that the planarization of two aryl planes in diarylureas may play a crucial role in cocrystallization. Also, a polymorph study bridged the transformation between these ureas and their DMSO complexes.

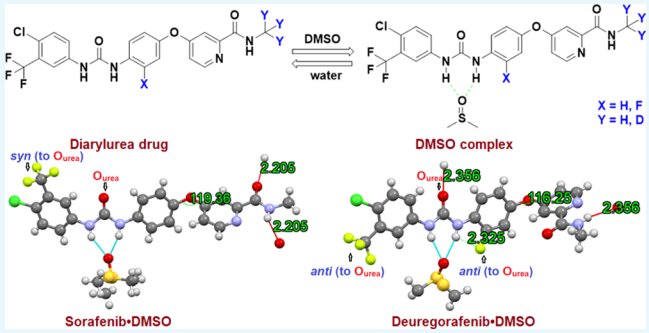

INTRODUCTION

Diarylureas are frequently used in self-assembly, anion recognition, and cocrystallization as they can act as both H-bond donors through their double NH units and acceptors by the urea C═O group.[1−4] Etter has summarized complexing rules for diphenylureas taking 1,3-bis(*m*-nitrophenyl)urea as the model substrate in the early 1990s.[5,6] The major conclusion is that diarylureas with strong meta-substituted electron-withdrawing substituents have the property to bond with strong acceptor solvents or reagents such as dimethyl sulfoxide (DMSO) and triphenylphosphine oxide (TPPO) in a 1:1 stoichiometry.[6−8] Later studies found that diarylureas could also recognize various anions including acid radicals, halides, and metal ions.[9−14] Yamasaki et al. recently reported the formation of a diphenylurea cocrystal between different diphenylureas.[15] In addition, the introduction of heteroaromatic substitutions (e.g., pyridine)[16,17] and more H-bond donors or acceptors (e.g., NO_2, pyrrole, I, F)[18−21] in aromatic units would afford more diverse packing patterns. At the same time, Nanjia, Swift, and co-workers made great efforts to predict the cocrystallization and possible assembly styles from substitution environment, electronic effects, and with the help of computational energy calculation.[8,15−17,22,23]

Urea is also a popular building block in the field of new drug discovery due to its stable H-bonding with a variety of target proteins or receptors.[24,25] In the past 2 decades, several urea-containing drugs have been approved, for example, sorafenib, regorafenib, ritonavir, and lenvatinib, and more candidates are in clinical or preclinical studies. The solvation of active pharmaceutical ingredients (APIs) could offer benefits on physicochemical properties, so it has gradually become an attractive strategy in drug design and polymorph screening.[26,27] So far, several drugs as solvates covering ethanolate, acetone, and DMSO complexes have been approved.[28−30] Cumulative research on the complexation of diarylureas with strong acceptors suggest that the solvation of urea-containing drugs is a feasible direction. DMSO is an ideal solvent since it has at least three advantages: (a) high safety, (b) a strong proton acceptor, and (c) excellent solubility beneficial for overcoming the poor solubility for most urea derivatives.[31] Jagdev Singh et al. reported getting a sorafenib DMSO solvate in a 1:1 stoichiometry according to powder X-ray diffraction (PXRD) and thermogravimetric analysis (TGA) in a WO patent.[32] Another patent described the connection between regorafenib

Received: December 4, 2020
Accepted: February 11, 2021
Published: February 19, 2021

https://dx.doi.org/10.1021/acsomega.0c05908
ACS Omega 2021, 6, 5532−5547

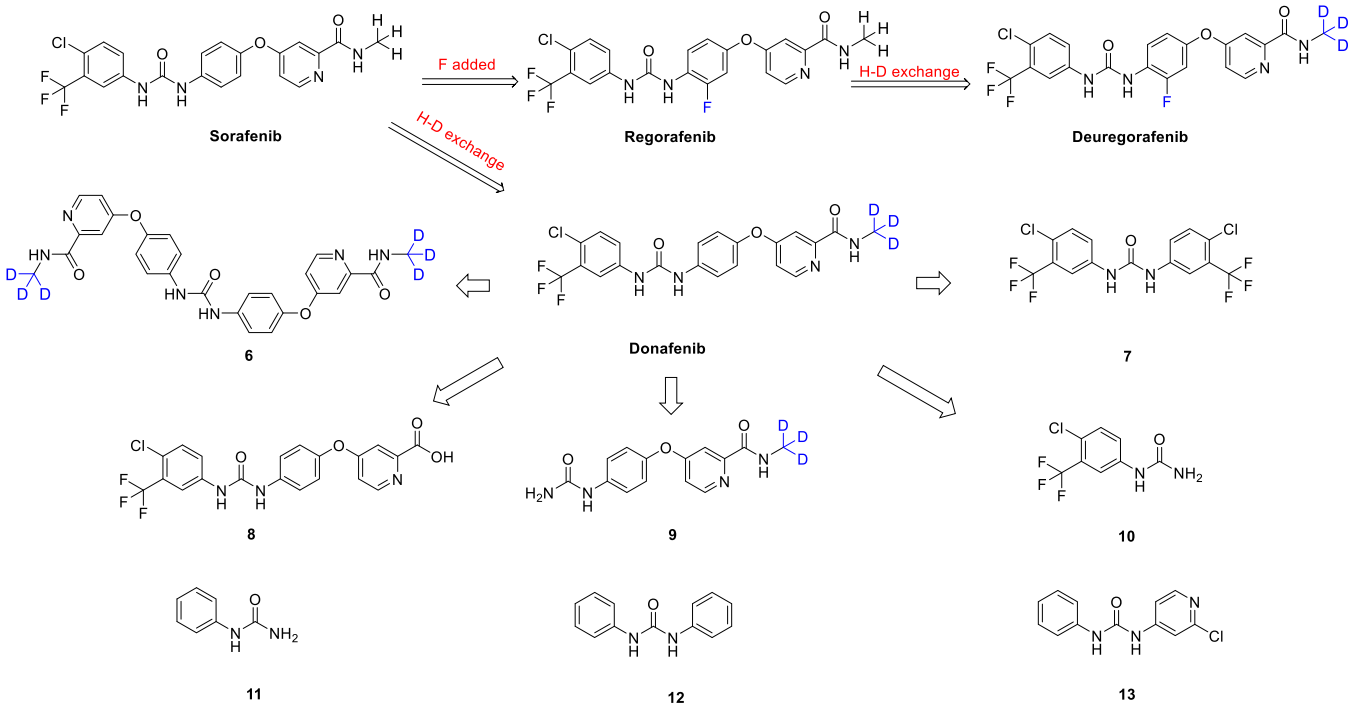

Figure 1. Diarylurea drugs and derivatives designed in this paper. Compounds **6**, **7**, **8**, **9**, and **10** are process impurities disassembled from donafenib while **11**, **12**, and **13** are commercially available.

Scheme 1. Route to Prepare Donafenib and Deuregorafenib from CD_3NH_2·HCl

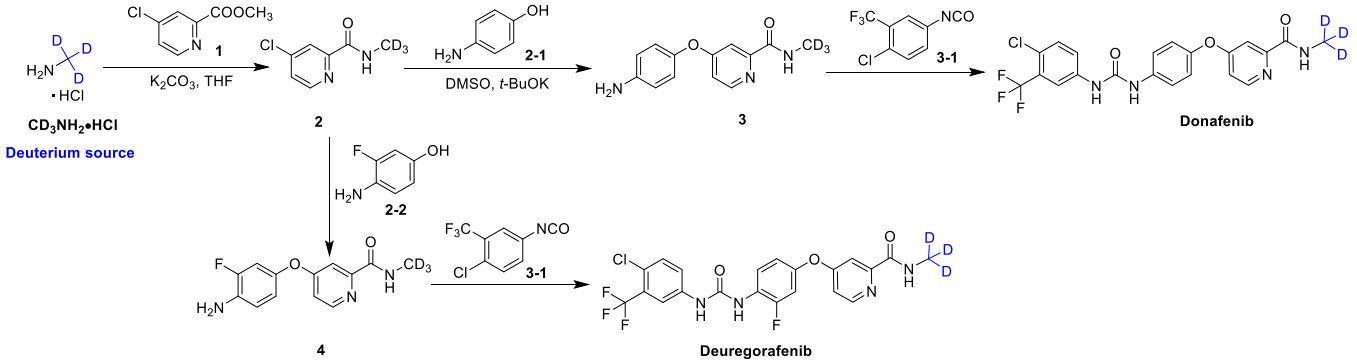

and DMSO without a complexing ratio.[33] Because of the lack of single crystals and more supporting data, the conclusion in both studies is inadequate. Unfortunately, except for these few general polymorph screening studies, research on the cooperation of diarylurea drugs with DMSO and related crystal structure is seldom reported. As the two best-selling drugs for cancer diseases for over 10 years, it is still unclear whether sorafenib and regorafenib could cocrystallize with DMSO. The possible bonding configuration, packing diversities before or after binding, and the influence of variant aromatic substituents on the crystal structure of corresponding DMSO cocrystals remain to be elucidated.

Donafenib (Figure 1) is a new generation of diphenylurea target kinase inhibitor deuterated from sorafenib proved to significantly improve overall survival (OS) with favorable safety and tolerability versus sorafenib.[34] We focus on this API together with the deuterated derivative of regorafenib named deuregorafenib. In view of the deuterated effect, four diarylurea molecules including sorafenib, donafenib, regorafenib, and deuregorafenib were included in our study at first. As the steric, substitution, and electronic effects all influence connection,[7,35−37] donafenib was disassembled and five related arylurea process impurities (**6**, **7**, **8**, **9**, and **10**) were added to the scope. Then, as a supplement to reach a conclusion, other three commercial arylureas (**11**, **12** and **13**) were also included. A general complexing procedure was developed, and it was applied to the above 12 designed substrates (Figure 1) for binding screening. Following attention focused on the single-crystal preparation for those successfully bonded cases, luckily five cocrystals were obtained from sorafenib, donafenib, deuregorafenib, **6**, and **7**. Crystal structures were carefully compared with reported parent motifs including sorafenib and regorafenib.[38−41] Several other disclosed simpler diarylureas and their DMSO solvates were also compared.[42,43] The molecular packing and stability were assessed from substitution effect and steric hindrance together with the relative lattice energy (ΔE_{latt}) calculation to rationalize observed similarities and diversities.

An element analysis (EA) issue on donafenib had been found by us a couple of years ago: the content of C and N for

https://dx.doi.org/10.1021/acsomega.0c05908
ACS Omega 2021, 6, 5532−5547

Scheme 2. Routes to Prepare 6, 7, 8, 9, and 10

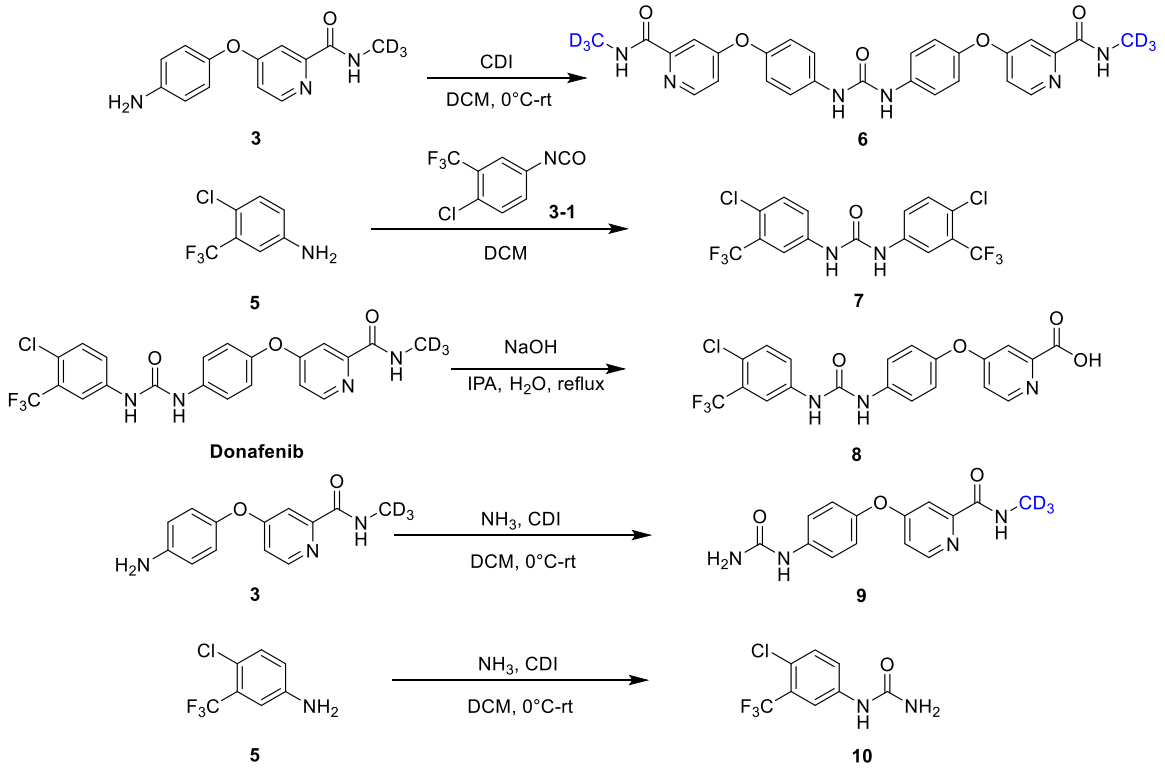

Scheme 3. Conversion between Donafenib and Donafenib·DMSO

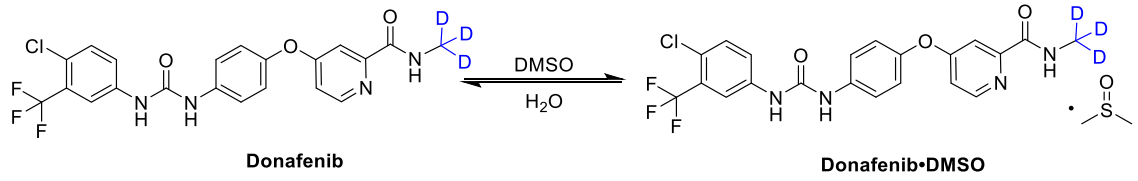

an earlier batch of donafenib separated from a binary solution of DMSO and water was lower than the theoretical value even after longer dryness. Later, nuclear magnetic resonance (NMR) investigation found the presence of a little DMSO, and we speculated that the formation of a small part of donafenib solvate may be the root cause. In this paper, a study on the polymorph transformation between these complexes and their parent polymorph was also performed through a water-test which was helpful to explain this EA issue.

EXPERIMENT SECTION

Materials. Methan-d_3-amine hydrochloride (CD_3NH_2·HCl) was supplied by Suzhou Zelgen Biopharmaceuticals Ltd. Co. and it was charged as the deuterium source to give donafenib and deuregorafenib, following a patented procedure[44] (Scheme 1). Five process impurities of donafenib (compounds **6**, **7**, **8**, **9**, and **10**) were prepared in Scheme 2. Sorafenib, regorafenib, **11**, **12**, **13**, and other commercial reagents or solvents were purchased and used directly.

Synthesis of Diarylureas and Corresponding DMSO Complexes. *Diarylureas.* The synthesis route for donafenib is outlined in Scheme 1: methyl 4-chloropicolinate (**1**) is converted to 4-chloro-*N*-(methyl-d_3)picolinamide (**2**) by amination with CD_3NH_2·HCl, following substitution reaction with 4-aminophenol (**2-1**) affords 4-(4-aminophenoxy)-*N*-(methyl-d_3)picolinamide (**3**). Donafenib forms after a final addition reaction with 1-chloro-4-isocyanato-2-(trifluoromethyl)benzene (**3-1**). Deuregorafenib could be achieved by a similar strategy by charging 4-amino-3-fluorophenol (**2-2**) instead of **2-1** in the substitution step. The self-condensation of **3** using *N*,*N*′-carbonyldiimidazole (CDI) gives compound **6**, and 4-chloro-3-(trifluoromethyl)-aniline (**5**) reacts with its corresponding isocyanate (**3-1**) to achieve **7**. The hydrolysis of donafenib in strong base provides **8**, and the coupling reaction between **3** or **5** with ammonia with the help of CDI affords **9** or **10** (Scheme 2). The detailed synthesis procedure for major diarylureas and intermediates is summarized in the Supporting Information; NMR spectra for three deuterated diarylureas are also included (Figures S1–S6).

Diarylurea DMSO Complexes. Take donafenib as an example; the scheme for preparing the corresponding DMSO complex is shown in Scheme 3. A general procedure was developed as follows: aryl−urea sample dissolves in DMSO with gentle heating; the resulting clear solution was then kept stirring with gradual cooling to room temperature, filtration under nitrogen until little filtrate dropped, and the resulting cake was subsequently dried in high vacuum at 50 °C to give the target complex.

Donafenib·DMSO. Donafenib (5.0 g) was added to DMSO (15 mL), and the mixture was stirred below 60 °C until

https://dx.doi.org/10.1021/acsomega.0c05908
ACS Omega 2021, 6, 5532−5547

completely dissolving under nitrogen protection. After cooling and filtration, the resulting cake was dried in vacuum at 50 °C for 48 h to afford the title compound as an off-white solid (4.1 g), yield: 70%. ^{1}H NMR (400 MHz, DMSO-d_6): δ 9.22 (s, 1H), 9.00 (s, 1H), 8.75 (s, 1H), 8.51 (d, J = 5.6 Hz, 1H), 8.13 (d, J = 2.4 Hz, 1H), 7.68−7.58 (m, 4H), 7.39 (d, J = 2.4 Hz, 1H), 7.20−7.14 (m, 3H), and 2.55 (s, 6H). ^{13}C NMR (100 MHz, DMSO-d_6): δ 166.43, 164.31, 152.95, 152.92, 150.85, 148.33, 139.79, 137.51, 132.47, 127.19 (q, J = 30.7 Hz), 123.60, 123.29 (q, J = 271.0 Hz), 122.85, 121.92, 121.01, 117.32 (q, J = 5.3 Hz), 114.49, 109.15, and 40.87. LCMS m/z: 468.27 [M−DMSO + H]$^+$ (ES$^+$) $C_{23}H_{19}D_3ClF_3N_4O_4S$ (545.98), calcd C 50.60, H 4.61, N 10.26; found, C 50.73, H 4.09, N 10.40.

To get the corresponding single crystals, a milligram scale of donafenib dissolved in DMSO mixed with a little water with gentle heating, filtration, and the sealed clear solution was kept at room temperature for days; colorless massive crystals were crystallized.

Sorafenib·DMSO. Separated as off-white solid. ^{1}H NMR (400 MHz, DMSO-d_6): δ 9.22 (s, 1H), 9.00 (s, 1H), 8.79−8.76 (m, 1H), 8.52 (d, J = 5.6 Hz, 1H), 8.13 (d, J = 2.4 Hz, 1H), 7.69−7.59 (m, 4H), 7.39 (d, J = 2.4 Hz, 1H), 7.20−7.15 (m, 3H), 2.80 (d, J = 4.8 Hz, 1H), and 2.55 (s, 6H). ^{13}C NMR (100 MHz, DMSO-d_6): δ 166.44, 164.26, 152.94, 150.84, 148.33, 139.81, 137.53, 132.47, 127.20 (q, J = 29.3 Hz), 123.60, 123.29 (q, J = 271.0 Hz), 122.82, 121.92, 121.00, 117.29 (q, J = 5.4 Hz), 114.49, 109.15, 40.92, and 26.47. LCMS m/z: 465.20 [M + H]$^+$ (ES$^+$) $C_{23}H_{22}ClF_3N_4O_4S$ (542.96), calcd. C 50.88, H 4.08, N 10.32; found, C 51.05, H 4.12, N 10.46.

In similar crystallization conditions as for donafenib·DMSO, colorless massive crystals were collected.

Deuregorafenib·DMSO. Separated as an off-white solid. ^{1}H NMR (400 MHz, DMSO-d_6): δ 9.53 (s, 1H), 8.75−8.73 (m, 2H), 8.54 (d, J = 5.6 Hz, 1H), 8.19 (t, J = 8.8 Hz, 1H), 8.13 (s, 1H), 7.66−7.61 (m, 2H), 7.46 (d, J = 2.4 Hz, 1H), 7.33 (dd, J = 2.8, 11.6 Hz, 1H), 7.19 (dd, J = 2.4, 5.6 Hz, 1H), 7.08 (dd, J = 1.2, 8.8 Hz, 1H), and 2.56 (s, 6H). ^{13}C NMR (100 MHz, DMSO-d_6): δ 165.93, 164.22, 153.20 (d, J_{CF} = 243.9 Hz), 153.03, 152.61, 150.91, 148.59 (d, J_{CF} = 10.1 Hz), 139.47, 132.52, 127.30 (q, J = 30.3 Hz), 125.39 (d, J_{CF} = 10.6 Hz), 123.39, 123.25 (q, J = 271.0 Hz), 123.09, 122.96, 117.51, 117.10 (q, J = 5.3 Hz), 114.57, 109.49 (d, J_{CF} = 21.7 Hz), 109.44, 40.91, and 25.63 (weak, CD_3). LCMS m/z: 486.25 [M + H]$^+$ (ES$^+$) $C_{23}H_{18}D_3ClF_4N_4O_4S$ (563.97), calcd. C 48.98, H 4.29, N 9.93; found, C 48.94, H 3.78, N 10.03.

Under similar crystallization conditions as for donafenib·DMSO, colorless needle-like crystals were obtained.

Regorafenib·DMSO. Separated as an off-white solid. ^{1}H NMR (400 MHz, DMSO-d_6): δ 9.53 (s, 1H), 8.79−8.73 (m, 2H), 8.54 (d, J = 5.6 Hz, 1H), 8.22 (t, J = 8.8 Hz, 1H), 8.14 (d, J = 1.6 Hz, 1H), 7.66−7.60 (m, 2H), 7.48 (d, J = 2.4 Hz, 1H), 7.32 (dd, J = 2.4, 11.6 Hz, 1H), 7.18 (dd, J = 2.4, 5.6 Hz, 1H), 7.08 (d, J = 8.8 Hz, 1H), 2.84 (d, J = 4.8 Hz, 1H), and 2.58 (s, 6H). ^{13}C NMR (100 MHz, DMSO-d_6): δ 165.92, 164.19, 153.13 (d, J_{CF} = 243.8 Hz), 153.01, 152.58, 150.86, 148.54 (d, J_{CF} = 10.2 Hz), 139.46, 132.47, 127.30 (q, J = 30.3 Hz), 125.41 (d, J_{CF} = 10.6 Hz), 123.32, 123.23 (q, J = 271.3 Hz), 123.09, 122.84, 117.46, 117.07 (q, J = 5.3 Hz), 114.53, 109.45, 109.42 (d, J_{CF} = 21.9 Hz), 40.88, and 26.42. LCMS m/z: 483.22 [M + H]$^+$ (ES$^+$) $C_{23}H_{21}ClF_4N_4O_4S$ (560.95), calcd C 49.25, H 3.77, N 9.99; found, C 49.36, H 3.76, N 10.08.

***6*·DMSO**. Separated as an off-white solid. ^{1}H NMR (400 MHz, DMSO-d_6): δ 8.92 (s, 2H), 8.78 (s, 2H), 8.55 (d, J = 5.6 Hz, 2H), 7.65 (d, J = 8.8 Hz, 4H), 7.44 (d, J = 2.8 Hz, 2H), 7.23−7.18 (m, 6H), and 2.59 (s, 6H). ^{13}C NMR (100 MHz, DMSO-d_6): δ 166.50, 164.32, 153.09, 152.92, 150.84, 147.98, 137.99, 121.94, 120.55, 114.44, 109.15, 40.89, and 25.58 (weak, CD_3). LCMS m/z: 519.39 [M + H]$^+$ (ES$^+$) $C_{29}H_{24}D_6N_6O_6S$ (596.69), calcd C 58.38, H 6.08, N 14.08; found, C 58.43, H 5.11, N 14.12.

Under similar crystallization conditions as for donafenib·DMSO, colorless plate crystals were obtained.

***7*·DMSO**. Separated as an off-white solid. ^{1}H NMR (400 MHz, DMSO-d_6): δ 9.33 (s, 2H), 8.09 (d, J = 2.0 Hz, 2H), 7.70−7.67 (m, 2H), 7.64−7.61 (m, 2H), and 2.55 (s, 6H). ^{13}C NMR (100 MHz, DMSO-d_6): δ 152.74, 139.35, 132.36, 127.21 (q, J = 30.4 Hz), 123.22 (q, J = 271.4 Hz), 123.81, 123.28, 117.58 (q, J = 5.4 Hz), and 40.84. LCMS m/z: 417.07 [M + H]$^+$ (ES$^+$) $C_{17}H_{14}Cl_2F_6N_2O_2S$ (495.26), calcd C 41.23, H 2.85, N 5.66; found, C 41.37, H 2.87, N 5.87.

Under similar crystallization conditions as for donafenib·DMSO, colorless needle-like crystals were obtained.

***8*·DMSO**. Separated as an off-white solid. ^{1}H NMR (400 MHz, DMSO-d_6): δ 12.89 (s, 1H), 9.28 (s, 1H), 9.06 (s, 1H), 8.58 (d, J = 5.6 Hz, 1H), 8.14 (d, J = 2.4 Hz, 1H), 7.69−7.61 (m, 4H), 7.44 (d, J = 2.4 Hz, 1H), 7.21−7.19 (m, 3H), and 2.56 (s, 6H). ^{13}C NMR (100 MHz, DMSO-d_6): δ 166.03, 165.37, 152.46, 150.59, 150.44, 147.67, 139.33, 137.19, 131.92, 126.71 (q, J = 30.4 Hz), 123.03, 122.79 (q, J = 271.0 Hz), 122.32, 121.36, 120.49, 116.80 (q, J = 5.7 Hz), 114.60, 111.80, and 40.39. LCMS m/z: 452.18 [M + H]$^+$ (ES$^+$) $C_{22}H_{19}ClF_3N_3O_5S$ (529.92), calcd C 49.86, H 3,61, N 7.93; found, C 49.97, H 3,68, N 8.12.

Solid obtained when **9**, **10**, **11**, or **12** was tried while following the above procedure contained little DMSO as shown in NMR. As for **13**, its solubility in DMSO is too high to form any precipitate. MS spectra for the above five cocrystals are reported in the Supporting Information (Figures S21−S25) in positive mode.

NMR Analysis Experiment. Whether a substrate could complex with DMSO or not can be quickly discriminated by NMR. DMSO-d_6 is used as a checking NMR solvent with a satisfactory resolution to DMSO. On the other hand, the great dissolving capacity of DMSO-d_6 is fit for these ureas. ^{1}H NMR and ^{13}C NMR are recorded on a Bruker AV400 MHz equipment. NMR also plays a crucial role in the polymorph transformation study.

IR Analysis Experiment. Fourier transform infrared (FT-IR) can also check the conversion between the parent urea and its DMSO complexes. All samples were run on a PerkinElmer spectrum two FT-IR spectrometer in the 400−4000 cm^{-1} region using a potassium bromide disk.

DSC and TGA Experiments. All differential scanning calorimetry (DSC) measurements were collected on a TA Instruments Q2000 DSC equipment at a heating rate of 10 °C/min from 30 to 300 °C. TGA was run on a Q500 TGA at a heating rate of 10 °C/min from 30 to 350 °C.

PXRD Experiment. PXRD was performed at room temperature on a Bruker D2 Phaser X-ray diffractometer. Data were collected and integrated over a 2θ = 3−45° with a step size of 0.02° using Bruker software.

Single-Crystal X-ray Diffraction Experiment. Single-crystal X-ray structures were collected on either a Bruker D8 Venture or Bruker SMART II CCD diffractometer using Mo

https://dx.doi.org/10.1021/acsomega.0c05908
ACS Omega 2021, 6, 5532−5547

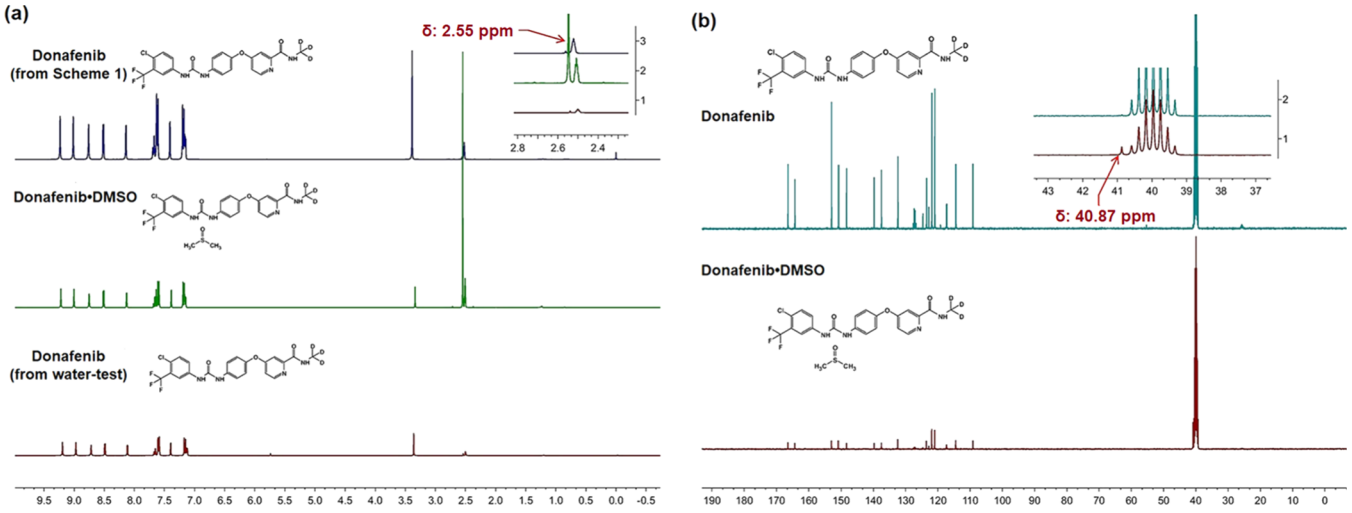

Figure 2. NMR comparison for donafenib and donafenib·DMSO in DMSO-d_6. (a) ^{1}H NMR comparison: donafenib from Scheme 1 (up), donafenib·DMSO (middle), and donafenib from donafenib·DMSO by water-test (down), δ_{DMSO} = 2.55 ppm. (b) ^{13}C NMR comparison: donafenib (up) and donafenib·DMSO (down), δ_{DMSO} = 40.87 ppm.

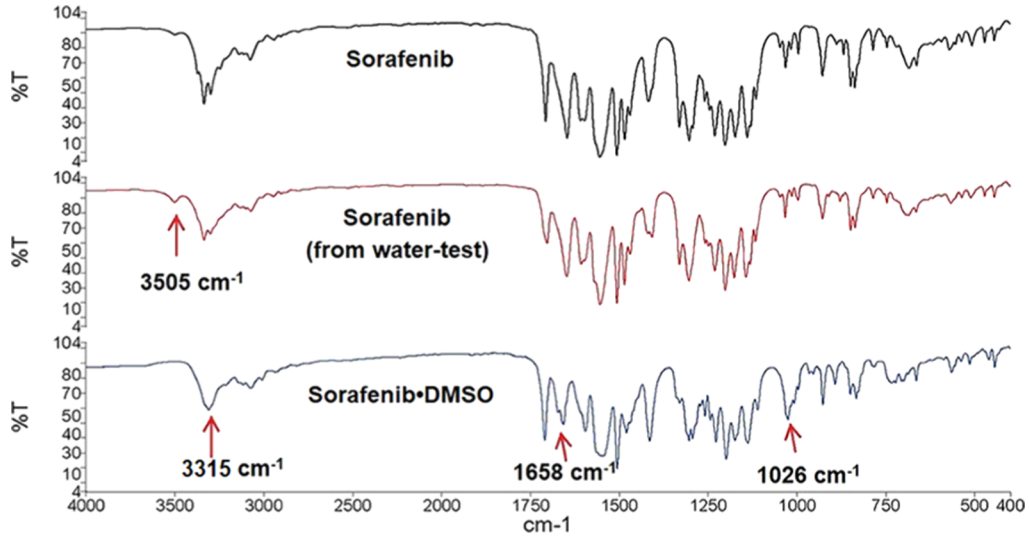

Figure 3. FT-IR spectrum comparison for sorafenib (black), sorafenib obtained from water-test (red), and sorafenib·DMSO (blue).

Kα or Cu Kα radiation at a set temperature between 150 and 296 K. All nonhydrogen atoms were solved using direct methods and refined by full matrix least-squares refinement on F^2 with anisotropic displacement parameters by SHELXL-97 followed by Mercury software for generation of the graphics for structural illustrations. All hydrogen atoms were placed by geometric calculation and difference Fourier map method. The overlap view for different structures was handled by Olex-2 software.

Polymorph Transformation Study by Water-Test. Five volumes of purified water were added to each complex with vigorous stirring at room temperature for hours, filtration, and adequate water-wash. The wet cake was dried in a high vacuum below 60 °C to afford the target solid which would be checked by NMR, infrared (IR), PXRD, or thermal analysis if necessary.

RESULTS AND DISCUSSION

NMR. Apparent DMSO methyl group peak occurred from both ^{1}H NMR and ^{13}C NMR spectra in cocrystallization test for donafenib, sorafenib, regorafenib, deuregorafenib, **6**, **7**, and **8**. The guest peak takes satisfactory resolution to that of DMSO-d_6 (δ_{DMSO} vs $\delta_{DMSO\text{-}d6}$: 2.55 ppm (singlet) versus 2.50 ppm (quintet) for ^{1}H NMR, 40.87 ppm (singlet) versus 39.52 ppm (septet) for ^{13}C NMR).[45] Calculated stoichiometric ratio of each host to DMSO is close to 1:1 from ^{1}H NMR. Trace DMSO is observed in the case of **9**, **10**, **11**, and **12**. For the polymorph transformation study, ^{1}H NMR of the solid from the water-test experiment shows little DMSO. The absence of DMSO confirms the smooth conversion between free diarylurea and its DMSO complexes. Taking donafenib as an example, Figure 2 presents the NMR comparison for donafenib, donafenib·DMSO, and the water-test sample from the complex. ^{1}H NMR and ^{13}C NMR spectrums for all seven DMSO complexes are summarized in the Supporting Information (Figures S7−S20).

Infrared Spectroscopy. Each DMSO complex more or less takes partly the difference from its parent phase from the FT-IR spectrum. Figure 3 illustrates the IR contrast images of sorafenib, sorafenib·DMSO, and the corresponding water-test sample; the major difference is around 3505, 3315, 1658, and

https://dx.doi.org/10.1021/acsomega.0c05908
ACS Omega 2021, 6, 5532−5547

Table 1. Crystallographic Data for Five DMSO Cocrystals

items	sorafenib·DMSO	donafenib·DMSO	deuregorafenib·DMSO	**6**·DMSO	7·DMSO
emp formula	$C_{21}H_{16}F_3ClN_4O_3·C_2H_6OS$[a]	$C_{21}H_{16}F_3ClN_4O_3·C_2H_6OS$[a]	$C_{21}H_{16}F_4ClN_4O_3·C_2H_6OS$[a]	$C_{27}H_{24}N_6O_5·C_2H_6OS$	$C_{15}H_8Cl_2F_6N_2O·C_2H_6OS$
formula weight	542.96	542.96	560.95	590.65	495.26
morph	colorless prism	colorless prism	colorless column	colorless plate	colorless prism
crystal system	monoclinic	monoclinic	monoclinic	monoclinic	orthorhombic
radiation type	Cu Kα	Cu Kα	Cu Kα	Cu Kα	Mo Kα
space group	*C*2/*c*	*C*2/*c*	$P2_1/n$	$P2_1/n$	*Pbcn*
T (K)	293(2)	296(2)	296(2)	296(2)	153(2)
a (Å)	26.892(5)	26.8958(4)	4.7798(10)	8.4185(2)	24.667(5)
b (Å)	9.1505(18)	9.14870(10)	25.2776(4)	27.7289(7)	13.077(3)
c (Å)	21.600(4)	21.6102(3)	20.8555(3)	12.6639(4)	25.283(5)
α (deg)	90.00	90.00	90.00	90.00	90.00
β (deg)	105.64(3)	105.6180(10)	90.610(10)	94.0510(10)	90.00
γ (deg)	90.00	90.00	90.00	90.00	90.00
vol (Å^3)	5118.5(18)	5121.11(12)	2519.66(8)	2948.82(14)	8156(3)
Z	8	8	4	4	16
calculated density	1.409 mg/m^3	1.408 mg/m^3	1.479 mg/m^3	1.330 mg/m^3	1.613 mg/m^3
crystal size	0.13 × 0.11 × 0.08 mm	0.24 × 0.12 × 0.11 mm	0.32 × 0.12 × 0.04 mm	0.40 × 0.12 × 0.06 mm	0.18 × 0.14 × 0.12 mm
$R_{(int)}$	0.0983	0.0347	0.0334	0.0245	0.0929
R_w	0.3079	0.1444	0.1494	0.1052	0.1503
absorption coefficient	2.609 mm^{-1}	2.608 mm^{-1}	2.729 mm^{-1}	1.419 mm^{-1}	0.492 mm^{-1}
independent reflections	4602	4571	4324	5205	8341
measured reflections	24037	14855	12442	19872	55874
CCDC deposition no.	2041748	2041747	2041750	2041749	2041751

[a]SC-XRD could not discriminate D and H, the "emp formula" and "formula weight" for the listed three deuterated cocrystals (donafenib·DMSO, deuregorafenib·DMSO, and **6**·DMSO) are recorded as nondeuterated styles. The corresponding presence of a deuterium atom is confirmed by NMR.

1026 cm^{-1}. The overlap view of IR for deuregorafenib and deuregorafenib·DMSO is presented in the Supporting Information (Figure S28).

Single-Crystal X-ray Diffraction. The cocrystallization possibility of designed arylureas with DMSO could be checked by NMR or IR preliminary, while the packing motif of the resulting cocrystals is clarified by single-crystal X-ray diffraction (SC-XRD). Crystallographic data for donafenib·DMSO, sorafenib·DMSO, deuregorafenib·DMSO, **6**·DMSO, and 7·DMSO is illustrated in Table 1. H-bonding parameters for five cocrystals are outlined in Table 2. Selected bond lengths, bond angles, and torsion angles [for C(O)−N−C−C_{meta}] are summarized in the Supporting Information (Tables S1−S3).

Sorafenib·DMSO. The ORTEP, ball-and-stick, and capped sticks views for sorafenib·DMSO are shown in Figure 4a−c. This colorless massive complex crystallizes in monoclinic space group *C*2/*c* with eight molecules in the unit cell. The crystal structure shows that one sorafenib molecule combines with one DMSO (partly in disorder) in bifurcated intermolecular H-bonding interaction, while the oxygen atom (O4) of DMSO accepts two urea NH (N1−H1A, N2−H2A) directly (2.16, 2.08 Å; 143.6, 146.3°) as a six-membered cyclic pattern. At the same time, another strong intermolecular H-bond forms between the host molecules, while O_{amide} (O3) directs to the NH_{amide} (N4−H4A) (2.21 Å, 144.8°) of a neighboring sorafenib molecule. In addition, intramolecular interactions including N−H···$N_{pyridine}$ (2.31 Å, 107.2°) and O_{urea}···H−C (*o*-phenyl) (2.32, 2.36 Å; 114.3, 116.3°) together with short contact between O_{urea} with adjacent C−H_{DMSO} (2.27 Å, 161.2°) both contribute to the stability of this cocrystal. The integrated interactions lead to a zigzag (9.15 Å) packing pattern for sorafenib·DMSO (Figure 4c).

Interestingly, when compared to the well-documented crystalline structure of sorafenib,[38] the CF_3 group in sorafenib·DMSO twists to a *syn*-conformation to urea C═O from *anti* (Figure 4d). This change can be attributed to the fact that this strong electron-withdrawing group can increase the acidity of the donor ortho C−H, strengthening the intramolecular C−H···O_{urea} interaction.[6,16,46] On the other hand, the *syn*-orientated CF_3 surrounds less steric hindrance which is beneficial for the inclusion of DMSO. Relative lattice energy (ΔE_{latt}) at zero Kelvin calculation is carried out by VASP software to assess the stability and rationality of possible computational simulated structures for sorafenib and related DMSO solvate (Table 3).[47] The ΔE_{latt} of sorafenib while CF_3 is in *syn*-conformation is 18.56 kJ/mol versus the *anti*-conformation case revealing that CF_3 in *anti*-conformation is more thermodynamically stable at 0 Kelvin which is just the reported crystalline structure. As for sorafenib·DMSO, the disordered DMSO (0.474:0.526) leads to two disordered types (type A and B, Figure 5a) resulting in four possible motifs, both cases while CF_3 is orientated to *syn*-position giving lower ΔE_{latt} (*syn* vs *anti*, type A: 0 vs 80.24 kJ/mol; type B: 8.30 vs 23.26 kJ/mol). In the *anti*-conformation case, the proximity of CF_3 groups in adjacent host molecules leads to obvious steric hindrance (Figure 5b). Hence, the packing motif in disordered type A with CF_3 locating in *syn* orientation is the most thermodynamically stable arrangement for sorafenib·DMSO.

Donafenib·DMSO. The ball-and-stick view for donafenib·DMSO is shown in Figure 6a. Few assembling diversities were observed in contrast to sorafenib·DMSO from the overlap view

https://dx.doi.org/10.1021/acsomega.0c05908
ACS Omega 2021, 6, 5532−5547

Table 2. H-Bonds Information for Five Cocrystals

cocrystals	D−H···A	*d* (D−H)/Å	*d* (H···A)/Å	*d* (D···A)/Å	angel (D−H···A)/°
donafenib·DMSO	N1−H1A···O4	0.86	2.18	2.918(3)	143.3
	N2−H2A···O4	0.86	2.09	2.842(3)	145.8
	N4−H4A···O3	0.91	2.14	2.949(2)	147.4
	C3−H3B···O1 (urea)	0.93	2.32	2.843(3)	114.8
	C9−H9A···O1 (urea)	0.93	2.34	2.880(3)	116.7
	N4−H4A···N3 (pyridine)	0.91	2.32	2.694(3)	103.9
sorafenib·DMSO	N1−H1A···O4	0.86	2.16	2.897(6)	143.6
	N2−H2A···O4	0.86	2.08	2.832(6)	146.3
	N4−H4A···O3	0.86	2.21	2.951(6)	144.8
	C3−H3B···O1 (urea)	0.93	2.32	2.833(7)	114.4
	C13−H13A···O1 (urea)	0.93	2.36	2.896(7)	116.1
	N4−H4A···N3 (pyridine)	0.86	2.31	2.695(7)	107.2
deuregorafenib·DMSO	N1−H1A···O4	0.86	2.07	2.883(3)	156.1
	N2−H2A···O4	0.86	2.07	2.874(3)	156.1
	N4−H4A···O1	0.86	2.36	3.025(3)	135.0
	C5−H5A···O1 (urea)	0.93	2.30	2.855(3)	118.1
	C13−H13A···O1 (urea)	0.93	2.26	2.847(3)	120.8
6·DMSO	N3−H3···O1′	0.86	2.09	2.904(18)	157.1
	N4−H4···O1′	0.86	2.14	2.953(2)	156.6
	N1−H1···O5	0.86	2.42	3.058(18)	131.8
	C2′−H2′A···O3	0.96	2.50	3.400(3)	155.6
	C7−H7···O4	0.93	2.61	3.184(2)	120.6
	C10−H10···O3	0.93	2.23	2.832(19)	121.9
	C16−H16···O3	0.93	2.23	2.830(2)	121.9
	C17−H17···O3	0.93	2.61	3.532(2)	170.0
	C22−H22···N2	0.93	2.63	3.501(19)	156.3
7·DMSO	N1−H1A···O2	0.88	2.00	2.839(4)	160.0
	N2−H2A···O2	0.88	2.10	2.920(4)	155.3
	N3−H3A···O4	0.88	2.01	2.848(4)	158.1
	N4−H4A···O4	0.88	2.02	2.856(4)	157.3
	C10−H10A···O1	0.95	2.21	2.837(4)	122.5
	C3−H3B···O1	0.95	2.23	2.855(4)	122.7
	C20−H20A···O3	0.95	2.26	2.875(4)	121.9
	C27−H27A···O3	0.95	2.23	2.853(4)	122.4

by Olex 2 software (Figure 6b). In detail, one donafenib molecule recognizes one DMSO (also in disorder) in bifurcated strong intermolecular interaction (2.09, 2.18 Å; 145.8, 143.3°) providing a similar six-membered ring. The O_{amide} accepts the NH_{amide} of an adjacent host (2.14 Å, 131.7°) leading to a similar zigzag pattern with CF_3 in *syn*-conformation to O_{urea}. The above two major intermolecular interactions direct the stability of this deuterated complex which is further strengthened by weaker intramolecular N−H···$N_{pyridine}$ (2.32 Å, 103.8°). Weak H-bonds between O_{urea} and CH (*o*-aryl), NH_{amide} and pyridine also exist. The great assembling consistent between donafenib·DMSO and sorafenib·DMSO suggests that D−H exchange would hardly disrupt the bonding interaction or packing motif for related DMSO complexes.

6·DMSO. The ORTEP, ball-and-stick, and capped sticks views for **6**·DMSO are presented in Figure 7a−c. As a deuterated symmetric donafenib process impurity, **6** cocrystallizes with DMSO as a colorless plate in a monoclinic crystal system with four molecules in the unit cell, and the space group is $P2_1/n$. To our astonishment, the O_{DMSO} (O1′) still receives the two urea NH (N4−H4, N3−H3) in a similar 6-membered cyclic intermolecular H-bonding interaction (2.09, 2.14 Å; 157.1, 156.6°), although no electron-withdrawing group substituted as donafenib or sorafenib, and the stoichiometry is maintained at 1:1 without any disorder. **6**·DMSO offers a counter-example to the cocrystallization rule of Etter.[6] This maybe associate with the two coplanar symmetrical aryl planes which could reduce the steric hindrance for the inclusion of DMSO. On the other hand, the symmetrical amides act as new H-bond donors (N1−H1) and acceptors (O5) to adjacent substrates (2.42 Å, 131.8°). Intermolecular interactions lead to a helical pattern (pitch: 27.7 Å) with anchored DMSO (Figure 7d). Owing to steric effects, C═O and N−H in the same amide unit cannot participate in H-bonding at the same time as donafenib. Moreover, the perfect coplanar [torsion angle (C(O)−N−C−C_{ortho}): −9.3(2)°, 171.30(15)°, 171.30(15)° and −7.2(3)°, see Table S3] promotes the weak intramolecular O_{urea}···H−C (*o*-aryl) in nearly the same length (2.23 Å). Integrating more diverse intermolecular and intramolecular H-bonding interactions contribute to the stability of this novel helical packing motif.

7·DMSO. **7** is another symmetric diarylurea process impurity of donafenib with two meta-substituted CF_3 groups. The ball-and-stick (Figure 8a) and capped sticks (Figure 8b) views for **7**·DMSO are illustrated. Greatly diverse from the other four complexes or reported solvates, **7**·DMSO crystallizes as a bis-molecular motif in orthorhombic space group *Pbcn* with 16 molecules in the unit cell. To the best of our knowledge, this is the first diarylurea DMSO complex with

https://dx.doi.org/10.1021/acsomega.0c05908
ACS Omega 2021, 6, 5532−5547

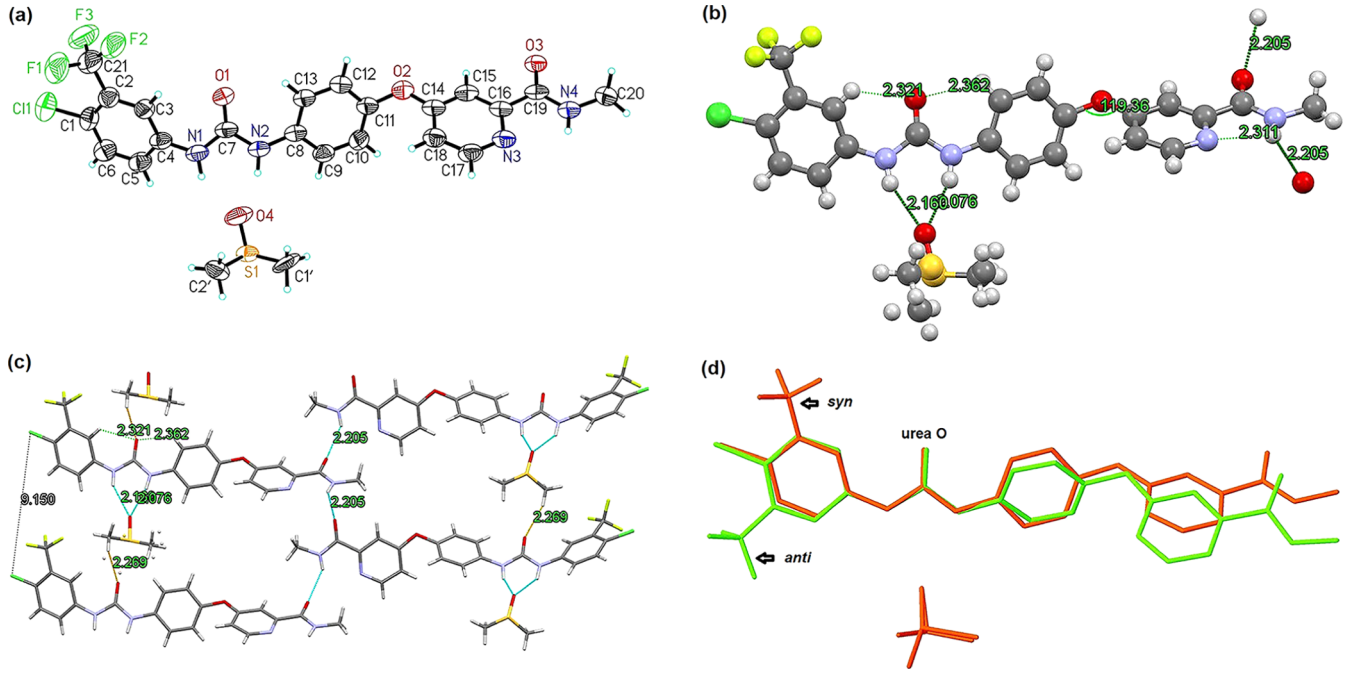

Figure 4. (a) ORTEP view for the asymmetric unit of sorafenib·DMSO. (b) Ball-and-stick view for sorafenib·DMSO: DMSO is in disorder and CF_3 is orientated *syn* to O_{urea}, H-bonds are shown as dashed lines. (c) Capped sticks view for sorafenib·DMSO as a zigzag pattern. (d) Overlap view for sorafenib·DMSO (red) and sorafenib (green, CCDC no.: 813502): CF_3 is orientated *anti* to O_{urea} in sorafenib.

Table 3. Relative Lattice Energy (ΔE_{latt}) for Simulated Structures of Sorafenib and Sorafenib·DMSO

Packing code	Structure	Orientation (CF_3 to O_{urea})	Disorder type	ΔE_{latt} (kJ/mol)
Sorafenib-1	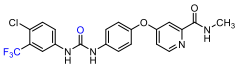	*anti*	NA	0
Sorafenib-2	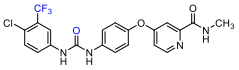	*syn*	NA	18.56[a]
Sorafenib•DMSO-A1	NA	*syn*	A	0
Sorafenib•DMSO-A2	NA	*anti*	A	80.24[b]
Sorafenib•DMSO-B1	NA	*syn*	B	8.30[b]
Sorafenib•DMSO-B2	NA	*anti*	B	23.26[b]

[a]Compared to sorafenib-1. [b]Compared to sorafenib·DMSO-A1.

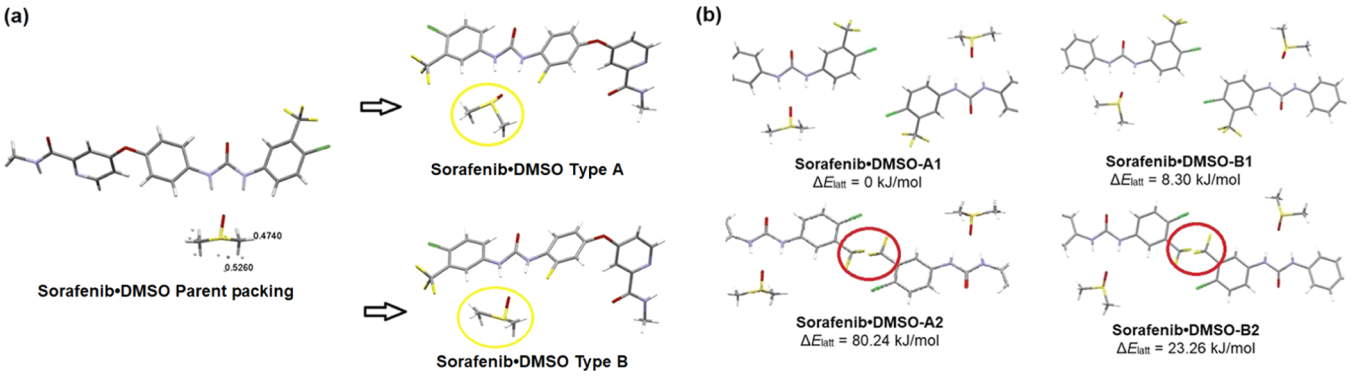

Figure 5. (a) Two disordered types in the crystalline motif of sorafenib·DMSO: type A and B (0.474:0.526). (b) Simulated structures for sorafenib·DMSO-A1 and sorafenib·DMSO-B1: (up) little steric hindrance; for sorafenib·DMSO-A2 and (down) sorafenib·DMSO-B2, obvious steric effects observed from neighboring CF_3.

Z = 16. Owing to the strong electron-withdrawing effect of CF_3, **7** smoothly accepts DMSO in similar six-membered H-bonding interaction (2.00, 2.10 Å/2.01, 2.02 Å; 160.0, 155.3°/158.1, 157.3°). Without pyridine or amide unit, the bonding interaction in **7**·DMSO is much simpler, and host molecules are bridged predominantly by van der Waals force. However, a significant off-set face-to-face $\pi-\pi$ stacking interaction between adjacent phenyl rings (3.674 and 3.698 Å, Figure 8b) forms.

https://dx.doi.org/10.1021/acsomega.0c05908
ACS Omega 2021, 6, 5532−5547

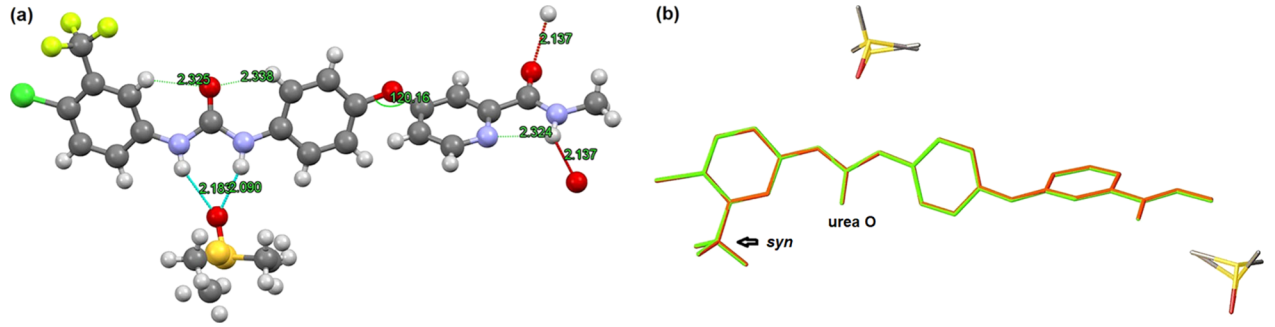

Figure 6. (a) Ball-and-stick view for donafenib·DMSO: DMSO is in disorder, H-bonds are shown as dashed lines. (b) Perfect overlap between Sonafenib·DMSO (green) and donafenib·DMSO (red) by Olex 2 software, both CF_3 are orientated *syn* to O_{urea}.

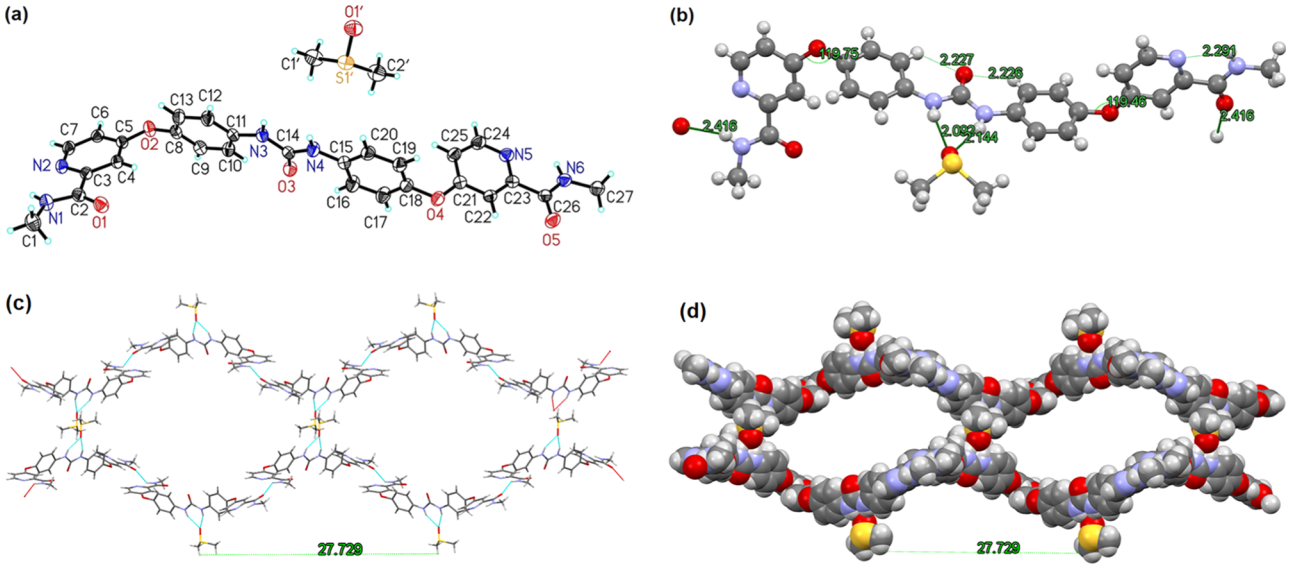

Figure 7. Diverse views for the asymmetric unit of **6**·DMSO. (a) ORTEP view, (b) ball-and-stick view with intermolecular ($N-H_{urea}\cdots O_{DMSO}$, $N-H_{amide}\cdots O_{amide}$) and intramolecular H−bonds ($O_{urea}\cdots H-C_{o\text{-}aryl}$, $N-H_{amide}\cdots N_{pyridine}$), (c) capped sticks view, and (d) spacefill view as a helix pattern: helical pitch = 27.7 Å. H-bonds are shown as dashed lines.

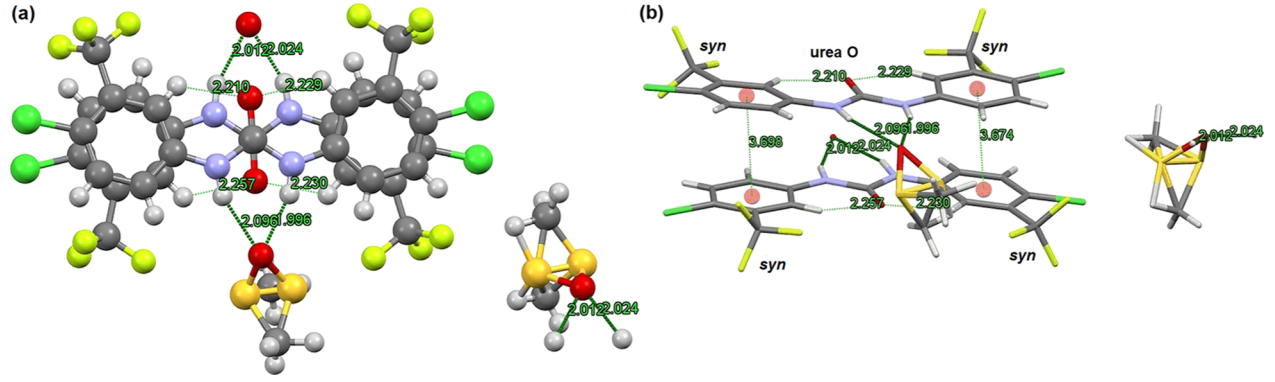

Figure 8. (a) Ball-and-stick view for **7**·DMSO as a bismolecule with two disordered DMSO, the orientation of both *m*-CF_3 is *syn* to O_{urea}; intermolecular ($N-H_{urea}\cdots O_{DMSO}$) and intramolecular H-bonds ($O_{urea}\cdots H-C_{o\text{-}phenyl}$) are shown as dashed lines. (b) Capped sticks view for **7**·DMSO as a paralleled pattern with obvious $\pi-\pi$ stacking interaction (3.674 and 3.698 Å).

Aryl rings are cross-arranged, which is beneficial for the packing stability from steric hindrance. In addition, weak intramolecular $C-H\cdots O_{urea}$ (C10−H10···O1, C3−H3···O1/C20−20···O3, C27−H27···O3; 2.21, 2.23 Å/2.26, 2.23 Å; 122.5, 122.7°/121.9, 122.4°) generates due to the electron-withdrawing effect from CF_3. Swift has noted that the relative stable orientation of meta-substituents for both mono- and bis meta-substitution is on the opposite side of O_{urea}.[7,8,23,37] However, both CF_3 in this case are orientated to the *syn*-conformation. This change could be rationalized by less steric and electronic effects superiority to strengthen the intramolecular $C-H\cdots O_{urea}$ by reducing the acidity of *ortho*-aryl C−H.

https://dx.doi.org/10.1021/acsomega.0c05908
ACS Omega 2021, 6, 5532−5547

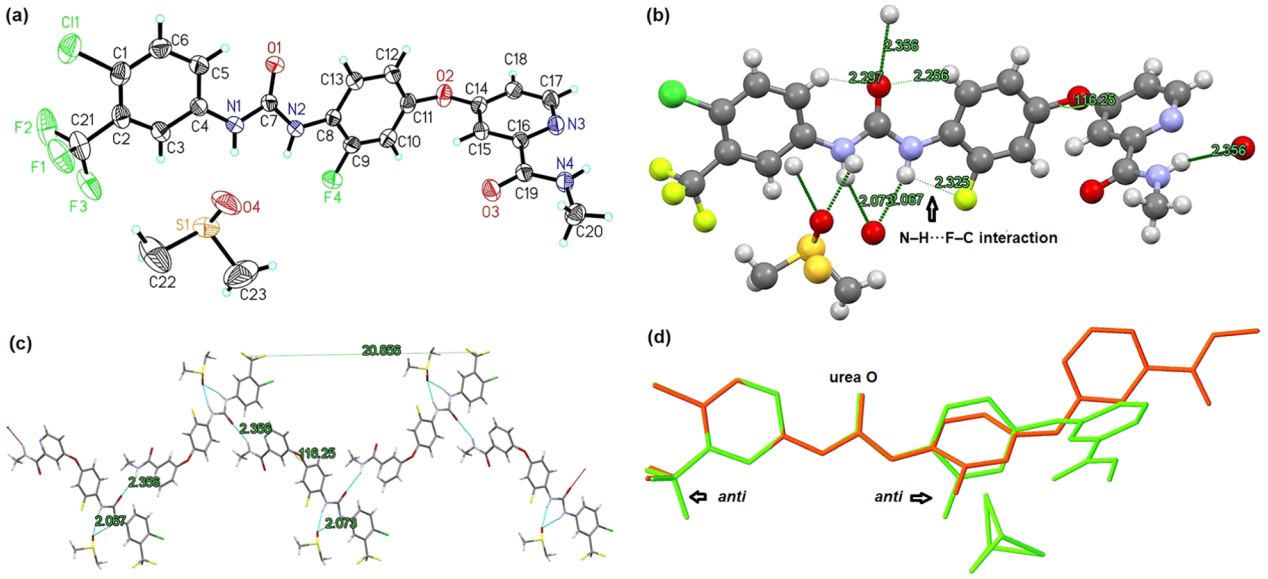

Figure 9. (a) ORTEP view for deuregorafenib·DMSO. Both orientations of *m*-CF_3 and *o*-F are *anti* to O_{urea}. (b) Ball-and-stick view for deuregorafenib·DMSO, DMSO partly in disorder. Intermolecular ($N-H_{urea}\cdots O_{DMSO}$, $N-H_{amide}\cdots O_{urea}$) and intramolecular H-bonds ($O_{urea}\cdots H-C_{o\text{-}aryl}$, $N-H_{amide}\cdots N_{pyridine}$) presented as dashed blue lines. (c) Capped sticks view, crystallized as a zigzag pattern. (d) Overlap view between doregorafenib·DMSO (green) and regorafenib (red) by Olex 2, F and CF_3 in both crystals in *anti*-orientation to O_{urea}, obvious twist for the pyridine unit.

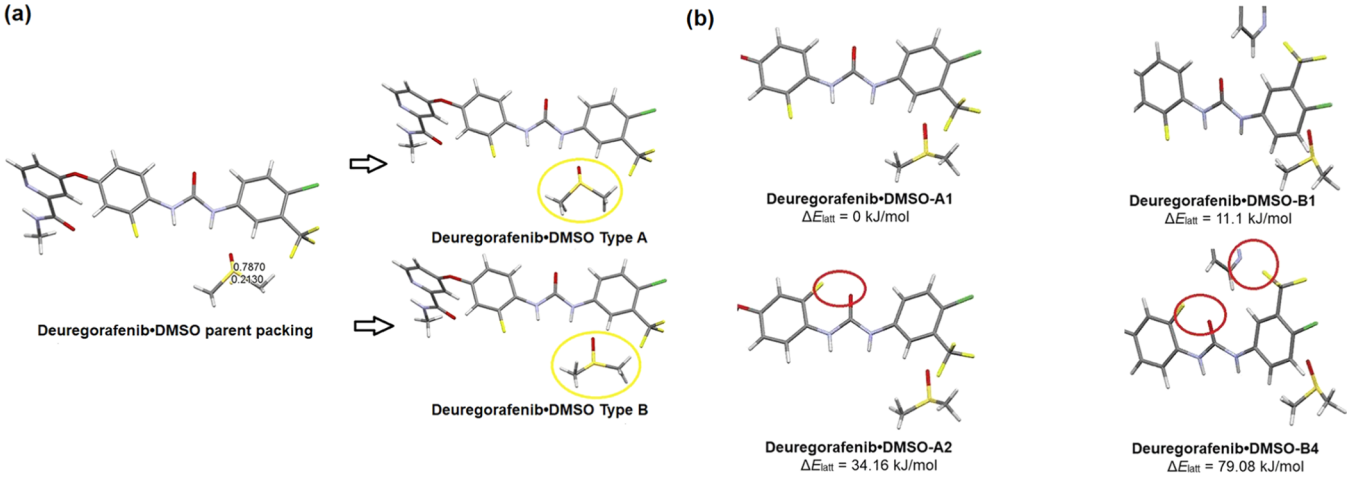

Figure 10. (a) Two disordered types in the crystalline motif of deuregorafenib·DMSO: type A and type B (0.787:0.213). (b) four selected simulated structures for deuregorafenib·DMSO, deuregorafenib·DMSO-A2 with obvious polarity repulsion between F atom and O_{urea}, and deuregorafenib·DMSO-B4 with both polarity repulsion between F and O_{urea}, CF_3 and $N_{pyridine}$.

Deuregorafenib·DMSO. An ortho F atom added to donafenib on the middle phenyl unit gives deuregorafenib. The ORTEP, ball-and-stick, and capped sticks views for deuregorafenib·DMSO are shown in Figure 9a–c. The crystal structure shows that F–H exchange will not disturb the arrangement of the above six-membered H-bonding pattern (2.07, 2.07 Å; 156.1, 156.1°) between deuregorafenib and DMSO (partly in disorder) in a stoichiometry of 1:1. By contrast, previous intermolecular $N-H_{amide}\cdots O_{urea}$ within adjacent host molecules in sorafenib·DMSO, donafenib·DMSO, and **6**·DMSO are absent. Instead, O_{urea} (O1) of one deuregorafenib accepts the NH_{amide} (N4–H4) of a neighboring host generating a new kind of H-bond (2.36 Å, 135.0°). This dramatic change is possible because of the bond angle of the aromatic ether structure (Figure 9b and Table S2) in deuregorafenib·DMSO [C14–O2–C11, 116.25 (18)°], smaller than that of sorafenib·DMSO [119.4 (5)°], donafenib·DMSO [120.16 (18)°], and **6**·DMSO [119.46 (12), 119.75 (12)°]. The decreased angle increases the steric hindrance for the previous direct amide H-bonding between host molecules. However, this change promotes the new formed H-bond. Directed by the two crucial intermolecular interactions, deuregorafenib·DMSO crystallizes as colorless needles in a monoclinic crystal system with four molecules in the unit cell, and the space group is $P2_1/n$.

The orientation study exhibits that CF_3 in this complex is in *anti* to O_{urea}. Moreover, the added F atom is also orientated to an *anti*-position. As we know, CF_3 in sorafenib, regorafenib, or regorafenib monohydrate all present *syn*-conformation.[38−41] To clarify, the relative lattice energy calculation simulated for regorafenib and deuregorafenib·DMSO was also performed, and corresponding contrasting data was outlined (Figure 10a,b

https://dx.doi.org/10.1021/acsomega.0c05908
ACS Omega 2021, 6, 5532−5547

Table 4. Relative Lattice Energy for Simulated Structures of Regorafenib and Deuregorafenib·DMSO

Packing code	Structure	Orientation (CF_3 to O_{urea})	Orientation (C–F to O_{urea})	Disorder Type	ΔE_{latt} (kJ/mol)
Regorafenib-1	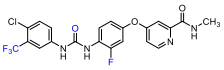	*anti*	*anti*	NA	0
Regorafenib-2	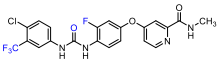	*anti*	*syn*	NA	7.14[a]
Regorafenib-3	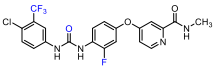	*syn*	*anti*	NA	28.89[a]
Regorafenib-4	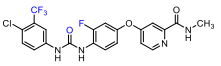	*syn*	*syn*	NA	42.59[a]
Deuregorafenib•DMSO-A1	NA	*anti*	*anti*	A	0
Deuregorafenib•DMSO-A2	NA	*anti*	*syn*	A	34.16[b]
Deuregorafenib•DMSO-A3	NA	*syn*	*anti*	A	43.89[b]
Deuregorafenib•DMSO-A4	NA	*syn*	*syn*	A	72.85[b]
Deuregorafenib•DMSO-B1	NA	*anti*	*anti*	B	11.1[b]
Deuregorafenib•DMSO-B2	NA	*anti*	*syn*	B	44.83[b]
Deuregorafenib•DMSO-B3	NA	*syn*	*anti*	B	48.87[b]
Deuregorafenib•DMSO-B4	NA	*syn*	*syn*	B	79.08[b]

[a]Compared to regorafenib-1. [b]Compared to deuregorafenib·DMSO-A1.

Table 5. Comparison of the Dihedral Angle of Two Aryl Planes in Diarylureas and Corresponding DMSO Complexes

entry	samples	dihedral angle	CCDC no.
1	sorafenib[38]	39.06°	813502
2	sorafenib·DMSO	28.05°	2041749
3	donafenib·DMSO	28.06°	2041747
4	regorafenib[40]	61.52°	1045583
5	deuregorafenib·DMSO	4.20°	2041750
6	1,3-bis(3-cyanophenyl)urea (β conformation)[7]	52.30°	1060065
7	1,3-bis(3-cyanophenyl)urea DMSO solvate[7]	22.08°	1060063
8	1-(4-iodophenyl)-3-(4-nitrophenyl)urea[26]	88.57°	231524
9	1-(4-iodophenyl)-3-(4-nitrophenyl)urea DMSO solvate[46]	9.18, 9.77°	676842
10	*N*-(4-methylphenyl)-4′-(4-nitrophenyl)urea[46]	86.79°	676850
11	*N*-(4-methylphenyl)-4′-(4-nitrophenyl)urea DMSO solvate[46]	18.97, 20.00°	676844

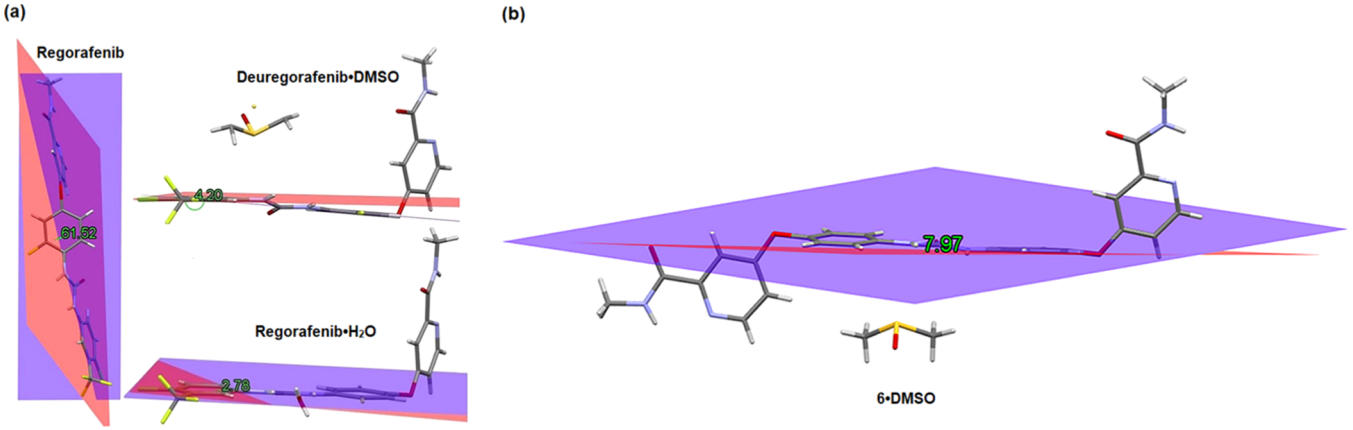

Figure 11. Dihedral angle of two aryl planes calculated by Mercury software. (a) regorafenib (61.52°), deuregorafenib·DMSO (4.20°), and regorafenib·H_2O (2.78°). (b) **6**·DMSO (7.97°).

and Table 4): both CF_3 and F in *anti*-conformation leads to the lowest ΔE_{latt} for four possible regorafenib motifs (0.00, 7.14, 28.89, and 42.59 kJ/mol). As for deuregorafenib·DMSO, although DMSO is partly in disorder (type A:type B = 0.787:0.213, Figure 10a), either case of CF_3 and F being in *anti*-conformation gives the lowest ΔE_{latt} (type A: 0.00 (deuregorafeniB·DMSO-A1 as standard, *anti*/*anti*), 34.16 (*anti*/*syn*), 43.89 (*syn*/*anti*), and 72.85 kJ/mol (*syn*/*syn*);

https://dx.doi.org/10.1021/acsomega.0c05908
ACS Omega 2021, 6, 5532−5547

type B: 11.1 (*anti*/*anti*), 4.83 (*anti*/*syn*), 48.87 (*syn*/*anti*) and 79.08 kJ/mol (*syn*/*syn*). Once CF_3 locates in *syn* position, repulsive interaction occurs between CF_3 and pyridine unit, and similar repulsion between F and O_{urea} generates if F is in *syn*-conformation. Repulsion interaction would decrease the packing stability. Another possible explanation for the orientation of F atom is associated with the reported weak N−H···F−C interaction (2.33 Å, Figure 9b) between neighboring NH_{urea} and the *ortho*-F.[28] Hence, although F−H exchange hardly affects the H-bonding pattern between the host and DMSO, it strongly influences the role of other donors or acceptors, giving a significant diverse structure to that of sorafenib or donafenib. A slight change in aromatic substituents indeed provides dramatic packing diversity for the cocrystals.[41]

Dihedral Angle of Two Aryl Planes. The great consistency of the crystal structure for sorafenib·DMSO and donafenib·DMSO suggests that D−H exchange could not influence the final arrangement. Based on this hypothesis, regorafenib·DMSO would present nearly the same assembling as deuregorafenib·DMSO. Packing comparison for more diarylureas and relevant DMSO complexes involving sorafenib with sorafenib·DMSO or donafenib·DMSO, regorafenib with deuregorafenib·DMSO, and other three combinations disclosed in the Cambridge Structural Database are summarized (Table 5).[7,26,38,40,46] Data cumulates that the dihedral angle of two aryl planes in most cases significantly decreases after the inclusion of DMSO (Figures S29−S30). Especially, the complex of regorafenib (61.52−4.20°, Figure 11a) or 1-(4-iodophenyl)-3-(4-nitrophenyl)urea (88.57−9.18, 9.77°) twists to roughly coplanar from the vertical state.[26,40,46] This coplanar results in more flexible self-assembly for host strengthening the intramolecular O···H−C (*o*-aryl). On the other hand, as a stronger H-bond acceptor with relative smaller volume, DMSO faces little steric effects to accept NH_{urea} as an adequate cavity is exposed with the help of planarization. Looking back on the counter-example of **6**·DMSO, the corresponding dihedral angle is 7.97° (Figure 11b) and the coplanar motif is fit for the inclusion of DMSO, although no electron-withdrawing groups are included.

Several other disclosed complexes bonded with water, TPPO, or THF also present a similar decrease in dihedral angles (Table 6, and Figure S31).[6,16,23,42,43] As a result, we believe that the planarization of two aryl planes in diarylureas plays a crucial role in the final cocrystallization.

Table 6. Comparison of the Dihedral Angles of Two Aryl Planes in Diarylureas and Related Diverse Cocrystals

entry	samples	dihedral angle	CCDC no.
1	regorafenib	61.52°	1045583
2	regorafenib·H_2O[40]	2.78°	1045581
3	1,3-bis(3-pyridyl)urea[16]	12.27°	270965
4	1,3-bis(3-pyridyl)urea dihydrate[16]	1.94°	270961
5	1,3-bis(*m*-nitrophenyl)urea[42]	87.79°	1259385
6	1,3-bis(m-nitrophenyl)urea monohydrate[43]	38.49°	291328
7	1,3-bis(m-nitrophenyl)urea tetrahydrofuran solvate[6]	5.48°	1168178
8	N,N′-bis[4-(trifluoromethyl)phenyl]urea23	87.77°	1554299
9	N,N′-bis[4-(trifluoromethyl)phenyl]urea oxo(triphenyl)-phosphane[23]	31.01°	1554307

PXRD, DSC, and TGA Experiments. Compared to the parent polymorph, the solid form of DMSO complexes take obvious different PXRD patterns which offer extra supporting data for the screened solvates (Figure 12c,d). PXRD obtained from SC-XRD simulation shows consistency with that of the scale-up sample following Scheme 3 in donafenib, and deuregorafenib indicates that the polymorph purity of solids from our general procedure is robust (Figures 12a,b and S27). Solids obtained from the water-test in the polymorph transformation study for the four drug complexes were also checked with PXRD, and each sample is consistent with the related free substrate (Figures 13a,b and S26). This result discloses the smooth desolvation from cocrystals with the help of water. Also, the compared PXRD pattern shows that the D-H exchange has little effect on the crystalline phase. The DSC endothermic peak for donafenib·DMSO is at 122.52 °C (Figure 14a) which is much lower than that of donafenib (210.39 °C, Figure 14c), and related weight loss from TGA (13.78%, calculated from 30 to 150 °C) is fit for the speculated 1:1 composition (Figure 14b, theory loss: 14.33%), while little weight loss happens in donafenib (Figure 14d).

Polymorph Transformation Study by Water-Test. Each solid from the water-test study by charging corresponding DMSO complex in water with stirring was checked by ^{1}H NMR (Figure 2). Consistently, the methyl peak of DMSO peak disappeared for all samples. Thesolid collected after water-test in the case of donafenib·DMSO was also analyzed with PXRD, proving the regeneration of its parent polymorph and that similar conversion happened to sorafenib·DMSO and deuregorafenib·DMSO. It revealed that the six-membered H-bonding interaction was disrupted quickly in water, and the released DMSO was washed over during workup. The smooth transformation between free diarylureas and their DMSO solvates offers a reasonable explanation for our EA issue, and it also confirms the case that few studies on anion recognition discovered cocrystallization between ureas and DMSO as a large amount of water was charged.[20,48−50]

Structure Scope for Forming DMSO Solvates to Diarylurea Drug Substances. The cocrystallization rule for this kind of 1:1 complexation has been summarized by Etter.[6] Several arylurea drug derivatives or analogues (**8**, **9**, **10**, **11**, **12**, and **13**) were also tried to clarify the structure scope of diarylurea drug substances. However, except for the complete diphenyl−urea sample **8**, free urea such as **9**, **10**, **11**, and nonsubstituted **12** failed to recognize DMSO, and **13** dissolves too smoothly in DMSO to give any precipitate. This result indicated that free urea may form unknown stronger H-bonds in the presence of an NH_2 unit. Thus, it seems that urea drugs with complete diarylurea unit are more likely to cocrystallize with DMSO.

CONCLUSIONS

In conclusion, the cocrystallization of some typical diarylurea drugs or their derivatives with the strong H-bond acceptor DMSO has been examined and analyzed. A scalable procedure for corresponding complexing with DMSO was developed with robust polymorph control. Five new obtained diffraction-quality cocrystals involving three deuterated samples present the 1:1 intermolecular six-membered cyclic H-bonding pattern between these drug-related molecules and DMSO consistently. Deuterium substitution hardly disrupts the complexing motif from sorafenib·DMSO and donafenib·DMSO, while F−H exchange leads to obvious assembling diversities in the case of

https://dx.doi.org/10.1021/acsomega.0c05908
ACS Omega 2021, 6, 5532−5547

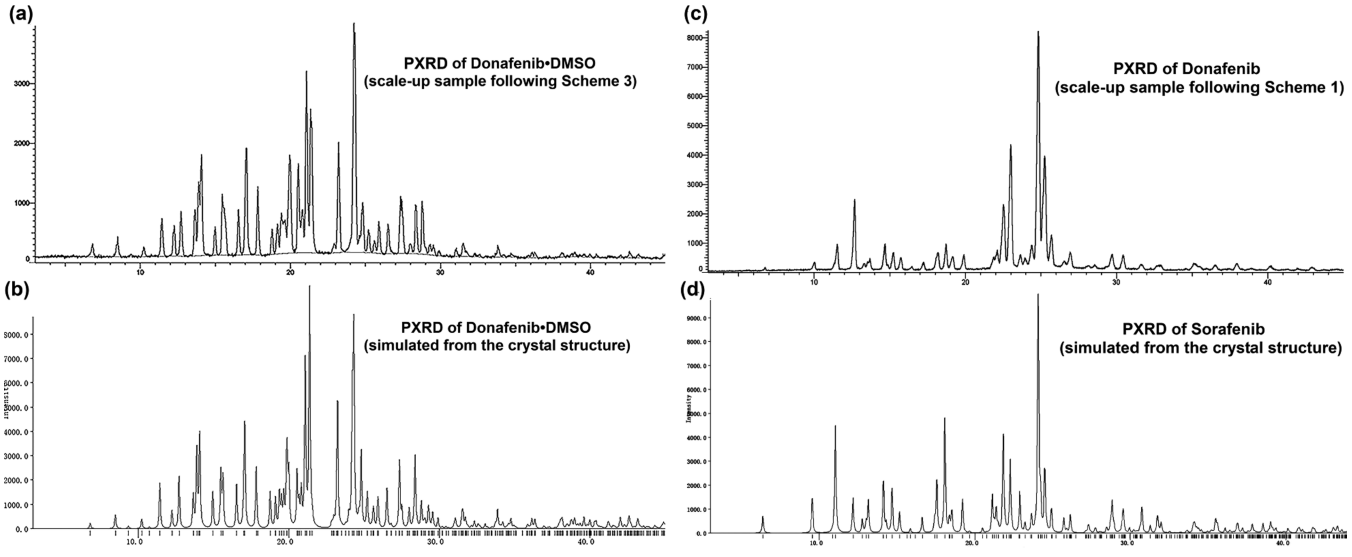

Figure 12. PXRD comparison between scale-up sample and simulated pattern from the crystal structure for donafenib·DMSO and donafenib. (a) Scale-up experimental pattern for donafenib·DMSO, (b) simulated pattern for donafenib·DMSO, (c) scale-up experimental pattern for donafenib, and (d) simulated pattern for sorafenib (CCDC no: 813502).

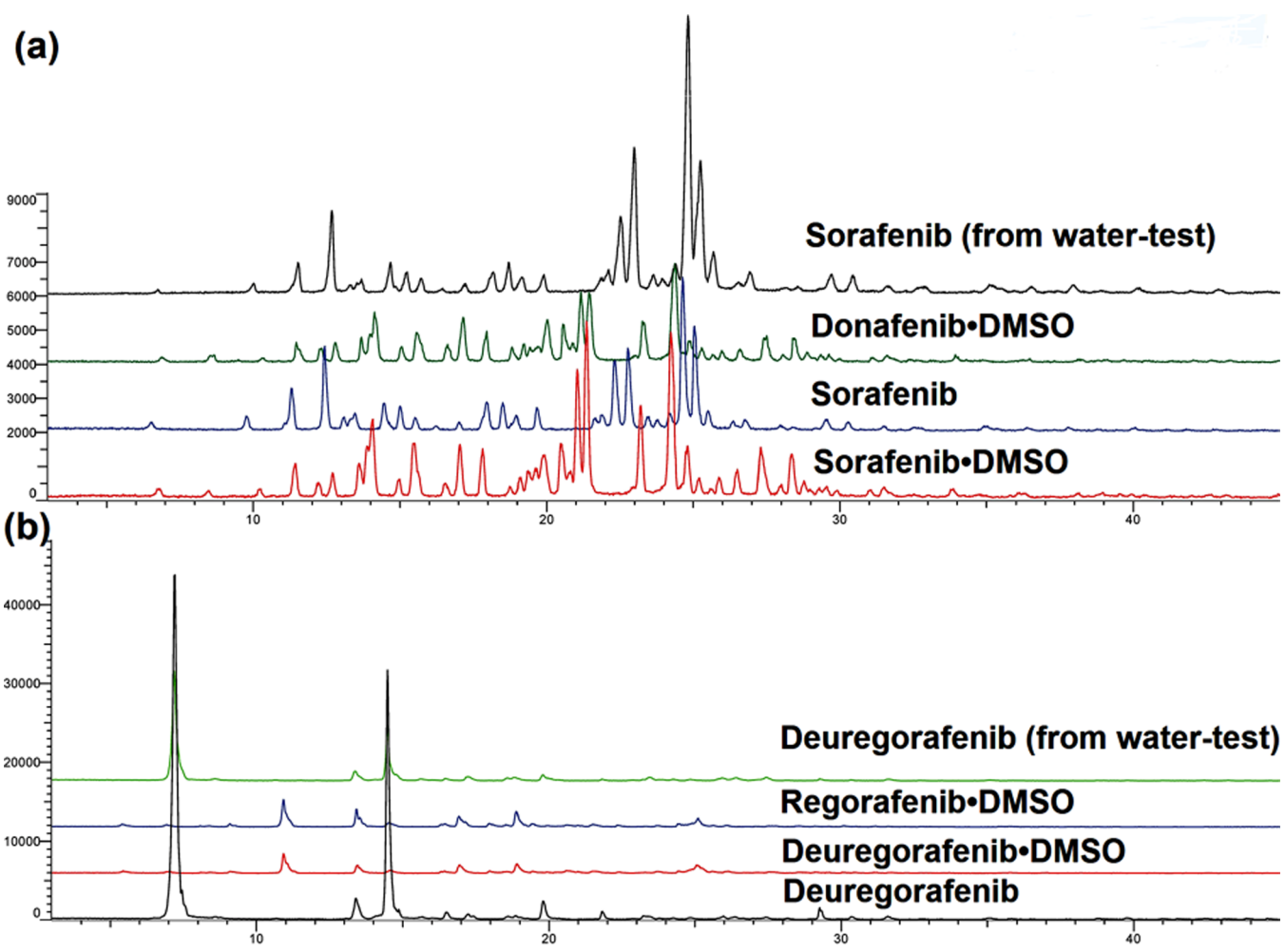

Figure 13. Overlay of PXRD spectra for cocrystallization and polymorph transformation studies. (a) Sorafenib·DMSO (red), sorafenib (blue), donafenib·DMSO (green), and sorafenib from the complex by water-test (black); donafenib·DMSO has a greatly similar PXRD pattern as that of sorafenib·DMSO. (b) Deuregorafenib (black), deuregorafenib·DMSO (red), regorafenib·DMSO, and deuregorafenib (green, from water-test).

deuregorafenib·DMSO. The complexing scope study showed that APIs without a complete diarylurea unit are difficult to cocrystallize. Although steric, substitution, and electronic effects indeed influence the orientation of meta- or ortho-

https://dx.doi.org/10.1021/acsomega.0c05908
ACS Omega 2021, 6, 5532−5547

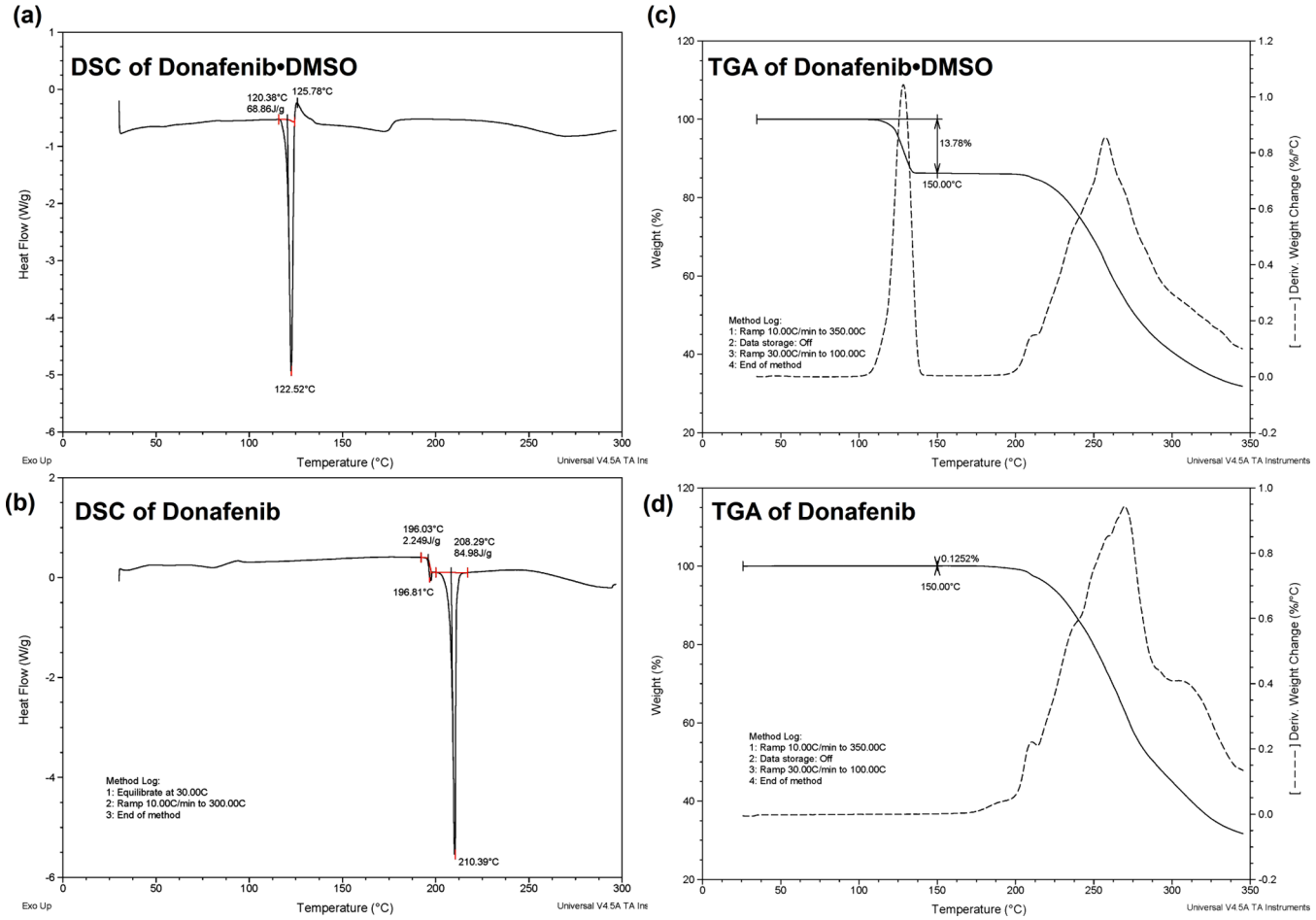

Figure 14. DSC and TGA spectra for donafenib·DMSO and donafenib. (a) DSC of donafenib·DMSO, endothermic peak: 122.52 °C. (b) TGA of donafenib·DMSO, weight loss: 13.78% (calculated from 30 to 150 °C). (c) DSC of donafenib, endothermic peak: 210.39 °C. (d) TGA of donafenib, weight loss: 0.1252% (calculated from 30 to 150 °C).

substituents, cumulated decreased dihedral angle data of two aryl planes either from our cocrystals or previous structures together with the counter-example of **6**·DMSO suggest that the planarization of two diarylurea planes may direct the inclusion of DMSO. Consistent desolvation of obtained complexes in water-test bridges the polymorph transformation between free diarylurea drugs and their DMSO complexes.

The findings on the cocrystallizing study of typical diarylurea drugs or derivatives with DMSO is helpful for new drug development and polymorph screening for urea-containing candidates,[51] and we will focus on and share possible pharmaceutical benefits such as the dissolution after complexing in the future.

■ ASSOCIATED CONTENT

Supporting Information

The Supporting Information is available free of charge at https://pubs.acs.org/doi/10.1021/acsomega.0c05908.

Preparation of major diarylureas and intermediates; spectroscopic characterization (^{1}H NMR, ^{13}C NMR, MS, IR, and PXRD) for complexes; and selected bond lengths, bond angles, torsion angles, and dihedral angles of two aryl planes (PDF)

Accession Codes

CCDC 2041747−2041751 contain the supplementary crystallographic data for this paper.

■ AUTHOR INFORMATION

Corresponding Authors

Binhua Lv − *Suzhou Zelgen Biopharmaceuticals Co., Limited, Kunshan, Jiangsu 215301, China*; Email: lvbh@zelgen.com

Youfu Luo − *State Key Laboratory of Biotherapy and Cancer Center, West China Hospital, West China Medical School, Sichuan University, Chengdu 610041, China*; orcid.org/0000-0001-7327-0368; Email: luo_youfu@scu.edu.cn

Authors

Chengwei Li − *State Key Laboratory of Biotherapy and Cancer Center, West China Hospital, West China Medical School, Sichuan University, Chengdu 610041, China; Suzhou Zelgen Biopharmaceuticals Co., Limited, Kunshan, Jiangsu 215301, China*

Jialiang Zhong − *Shanghai Institute of Pharmaceutical Industry, China State Institute of Pharmaceutical Industry, Shanghai 201203, China*

Baohu Liu − *Suzhou Zelgen Biopharmaceuticals Co., Limited, Kunshan, Jiangsu 215301, China*

Tao Yang − *State Key Laboratory of Biotherapy and Cancer Center, West China Hospital, West China Medical School, Sichuan University, Chengdu 610041, China*

https://dx.doi.org/10.1021/acsomega.0c05908
ACS Omega 2021, 6, 5532−5547

Complete contact information is available at:
https://pubs.acs.org/10.1021/acsomega.0c05908

Author Contributions

‖C.L. and J.Z. are contributed equally to this work.

Notes

The authors declare no competing financial interest.

■ ACKNOWLEDGMENTS

This research is supported by Suzhou Zelgen Biopharmaceuticals Co., Ltd. We thank Jiajun Huang and Zhuocen Yang (Shenzhen Jingtai Technology Co., Ltd.) for their help in the relative lattice energy calculation and Yanqing Gong (Shanghai Institute of Pharmaceutical Industry) for her assistance with data collection and refinement.

■ REFERENCES

(1) Fan, E.; Van Arman, S. A.; Kincaid, S.; Hamilton, A. D. Molecular recognition: hydrogen-bonding receptors that function in highly competitive solvents. *J. Am. Chem. Soc.* **1993**, *115*, 369−370.
(2) Gómez, D. E.; Fabbrizzi, L.; Licchelli, M.; Monzani, E. Urea vs. thiourea in anion recognition. *Org. Biomol. Chem.* **2005**, *3*, 1495−1500.
(3) Custelcean, R. Crystal engineering with urea and thiourea hydrogen-bonding groups. *Chem. Commun.* **2008**, 295−307.
(4) Gilday, L. C.; Robinson, S. W.; Barendt, T. A.; Langton, M. J.; Mullaney, B. R.; Beer, P. D. Halogen bonding in supramolecular chemistry. *Chem. Rev.* **2015**, *115*, 7118−7195.
(5) Etter, M. C.; Panunto, T. W. 1,3-Bis(*m*-nitrophenyl)urea: an exceptionally good complexing agent for proton acceptors. *J. Am. Chem. Soc.* **1988**, *110*, 5896−5897.
(6) Etter, M. C.; Urbanczyk-Lipkowska, Z.; Zia-Ebrahimi, M.; Panunto, T. W. Hydrogen bond-directed cocrystallization and molecular recognition properties of diarylureas. *J. Am. Chem. Soc.* **1990**, *112*, 8415−8426.
(7) Capacci-Daniel, C. A.; Mohammadi, C.; Urbelis, J. H.; Heyrana, K.; Khatri, N. M.; Solomos, M. A.; Swift, J. A. Structural diversity in 1,3-bis(*m*-cyanophenyl)urea. *Cryst. Growth Des.* **2015**, *15*, 2373−2379.
(8) Solomos, M. A.; Mohammadi, C.; Urbelis, J. H.; Koch, E. S.; Osborne, R.; Usala, C. C.; Swift, J. A. Predicting Cocrystallization Based on Heterodimer Energies: The Case of N,N′-Diphenylureas and Triphenylphosphine Oxide. *Cryst. Growth Des.* **2015**, *15*, 5068−5074.
(9) Calderon-Kawasaki, K.; Kularatne, S.; Li, Y. H.; Noll, B. C.; Scheidt, W. R.; Burns, D. H. Synthesis of Urea Picket Porphyrins and Their Use in the Elucidation of the Role Buried Solvent Plays in the Selectivity and Stoichiometry of Anion Binding Receptors. *J. Org. Chem.* **2007**, *72*, 9081−9087.
(10) Dial, B. E.; Rasberry, R. D.; Bullock, B. N.; Smith, M. D.; Pellechia, P. J.; Profeta, S., Jr.; Shimizu, K. D. Guest-accelerated molecular rotor. *Org. Lett.* **2011**, *13*, 244−247.
(11) Gillen, D. M.; Hawes, C. S.; Gunnlaugsson, T. Solution-state anion recognition, and structural studies, of a series of electron-rich *meta*-phenylene bis(phenylurea) receptors and their self-assembled structures. *J. Org. Chem.* **2018**, *83*, 10398−10408.
(12) Pfeifer, L.; Engle, K. M.; Pidgeon, G. W.; Sparkes, H. A.; Thompson, A. L.; Brown, J. M.; Gouverneur, V. Hydrogen-bonded homoleptic fluoride-diarylurea complexes: structure, reactivity, and coordinating power. *J. Am. Chem. Soc.* **2016**, *138*, 13314−13325.
(13) Custelcean, R.; Moyer, B. A.; Bryantsev, V. S.; Hay, B. P. Anion Coordination in Metal−Organic Frameworks Functionalized with Urea Hydrogen-Bonding Groups. *Cryst. Growth Des.* **2006**, *6*, 555−563.
(14) Jia, C.; Zuo, W.; Zhang, D.; Yang, X.-J.; Wu, B. Anion recognition by oligo-(thio)urea-based receptors. *Chem. Commun.* **2016**, *52*, 9614−9627.
(15) Yamasaki, R.; Iida, M.; Ito, A.; Fukuda, K.; Tanatani, A.; Kagechika, H.; Masu, H.; Okamoto, I. Crystal Engineering of N,N′-Diphenylurea Compounds Featuring Phenyl-Perfluorophenyl Interaction. *Cryst. Growth Des.* **2017**, *17*, 5858−5866.
(16) Reddy, L. S.; Basavoju, S.; Vangala, V. R.; Nangia, A. Hydrogen Bonding in Crystal Structures ofN,N′-Bis(3-pyridyl)urea. Why Is the N−H···O Tape Synthon Absent in Diaryl Ureas with Electron-Withdrawing Groups? *Cryst. Growth Des.* **2006**, *6*, 161−173.
(17) Todd, A. M.; Anderson, K. M.; Byrne, P.; Goeta, A. E.; Steed, J. W. Helical or Polar Guest-DependentZ′ = 1.5 orZ′ = 2 Forms of a Sterically Hindered Bis(urea) Clathrate. *Cryst. Growth Des.* **2006**, *6*, 1750−1752.
(18) George, S.; Nangia, A.; Lam, C.-K.; Mak, T. C. W.; Nicoud, J.-F. Crystal engineering of urea α-network via I···O2N synthon and design of SHG active crystal N-4-iodophenyl-N′-4′-nitrophenylurea. *Chem. Commun.* **2004**, *52*, 1202−1203.
(19) Abad, A.; Agulló, C.; Cuñat, A. C.; Vilanova, C.; Ramírez de Arellano, M. C. X-ray Structure of FluorinatedN-(2-Chloropyridin-4-yl)-N′-phenylureas. Role of F Substitution in the Crystal Packing. *Cryst. Growth Des.* **2006**, *6*, 46−57.
(20) Tarai, A.; Baruah, J. B. Conformation and visual distinction between urea and thiourea derivatives by an acetate ion and a hexafluorosilicate cocrystal of the urea derivative in the detection of water in dimethylsulfoxide. *ACS Omega* **2017**, *2*, 6991−7001.
(21) Nayak, B.; Halder, S.; Das, G. Terminal substituent induced differential anion coordination and self-assembly: case study of flexible linear bis-urea receptors. *Cryst. Growth Des.* **2019**, *19*, 2298−2307.
(22) Cabeza, A. J. C.; Day, G. M.; Motherwell, W. D. S.; Jones, W. Prediction and observation of isostructurality induced by solvent incorporation in multicomponent crystals. *J. Am. Chem. Soc.* **2006**, *128*, 14466−14467.
(23) Solomos, M. A.; Watts, T. A.; Swift, J. A. Predicting cocrystallization based on heterodimer energies: part II. *Cryst. Growth Des.* **2017**, *17*, 5073−5079.
(24) Sikka, P.; Sahu, J. K.; Mishra, A. K.; Hashim, S. R. Role of aryl urea containing compounds in medicinal chemistry. *Med. Chem.* **2015**, *5*, 479−483.
(25) Ghosh, A. K.; Brindisi, M. Urea derivatives in modern drug discovery and medicinal chemistry. *J. Med. Chem.* **2020**, *63*, 2751−2788.
(26) Salorinne, K.; Lahtinen, T.; Marjomäki, V.; Häkkinen, H. Polymorphic and solvate structures of ethyl ester and carboxylic acid derivatives of WIN 61893 analogue and their stability in solution. *CrystEngComm* **2014**, *16*, 9001−9009.
(27) Näther, C.; Jess, I.; Seyfarth, L.; Bärwinkel, K.; Senker, J. Trimorphism of betamethasone valerate: preparation, crystal structures, and thermodynamic relations. *Cryst. Growth Des.* **2015**, *15*, 366−373.
(28) https://www.ema.europa.eu/en/documents/scientific-discussion/crixivan-epar-scientific-discussion_en.pdf (accessed April 12, 2020).
(29) https://www.ema.europa.eu/en/documents/assessment-report/jevtana-epar-public-assessment-report_en.pdf (accessed April 12, 2020).
(30) https://www.ema.europa.eu/en/documents/assessment-report/mekinist-epar-public-assessment-report_en.pdf (accessed April 12, 2020).
(31) Brychczynaska, M.; Davey, R. J.; Pidcock, E. A study of dimethylsulfoxide solvates using the Cambridge structural database (CSD). *CrystEngComm* **2012**, *14*, 1479−1484.
(32) Jagdev Singh, J.; Swargam, S.; Rajesh Kumar, T.; Mohan, P.; Deorao, Z. S.; Shankar, S. A. 4-(4-{3-[4-chloro-3-(trifluoromethyl)-phenyl]ureido}phenoxy)-N^2-methylpyridine-2-carboxamide dimethyl sulphoxide solvate. WO 2011092663 A2, August 4, 2011.
(33) Srinivasan, T. R.; Sajja, E.; Gutta, M. Process for the preparation of 4-[4-({[4-chloro-3-trifluoromethyl)phenyl]-carbamoyl}amino)-3-fluoxophenoxy]-*N*-methylpyridine-2-carboxamide and its polymorphs thereof. WO 2016051422 A2, April 7, 2016.

(34) Bi, F.; Qin, S.; Gu, S.; Bai, Y.; Chen, Z.; Wang, Z.; Ying, J.; Lu, Y.; Meng, Z.; Pan, H.; Yang, P.; Zhang, H.; Chen, X.; Xu, A.; Liu, X.; Meng, Q.; Wu, L.; Chen, F. Donafenib versus sorafenib as first-line therapy in advanced hepatocellular carcinoma: An open-label, randomized, multicenter phase II/III trial. *J. Clin. Oncol.* **2020**, *38*, 4506.
(35) Brooks, S. J.; Gale, P. A.; Light, M. E. Ortho-phenylenediamine bis-urea-carboxylate: a new reliable supramolecular synthon. *CrystEngComm* **2005**, *7*, 586−591.
(36) Capacci-Daniel, C.; Dehghan, S.; Wurster, V. M.; Basile, J. A.; Hiremath, R.; Sarjeant, A. A.; Swift, J. A. Halogen/methyl exchange in a series of isostructural 1,3-bis(m-dihalophenyl)ureas. *CrystEngComm* **2008**, *10*, 1875−1880.
(37) Solomos, M. A.; Watts, T. A.; Swift, J. A. Ortho-substituent effects on diphenylurea packing motifs. *Cryst. Growth Des.* **2017**, *17*, 5065−5072.
(38) Ravikumar, K.; Sridhar, B.; Rao, A. K. S. B.; Reddy, M. P. Sorafenib and its tosylate salt: a multikinase inhibitor for treating cancer. *Acta Crystallogr., Sect. C: Cryst. Struct. Commun.* **2011**, *C67*, 29−32.
(39) Yang, P.; Qin, C.; Du, S.; Jia, L.; Qin, Y.; Gong, J.; Wu, S. Crystal Structure, Stability and Desolvation of the Solvates of Sorafenib Tosylate. *Crystals* **2019**, *9*, 367.
(40) Sun, M.-Y.; Wu, S.-X.; Zhou, X.-B.; Gu, J.-M.; Hu, X.-R. Comparison of the crystal structures of the potent anticancer and anti-angiogenic agent regorafenib and its monohydrate. *Acta Crystallogr., Sect. C: Cryst. Struct. Commun.* **2016**, *72*, 291−296.
(41) Liu, C.; Xu, C.-Q.; Yu, J.; Pui, Y.; Chen, H.; Wang, S.; Zhu, A. D.; Li, J.; Qian, F. Impact of a single hydrogen substitution by fluorine on the molecular interaction and miscibility between sorafenib and polymers. *Mol. Pharm.* **2019**, *16*, 318−326.
(42) Huang, K.-S.; Britton, D.; Etter, M. C.; Byrn, S. R. Polymorphic characterization and structural comparisons of the non-linear optically active and inactive forms of two polymorphs of 1,3-bis(*m*-nitrophenyl)urea. *J. Mater. Chem.* **1995**, *5*, 379−383.
(43) Rafilovich, M.; Bernstein, J.; Harris, R. K.; Apperley, D. C.; Karamertzanis, P. G.; Price, S. L. Groth's Original Concomitant Polymorphs Revisited. *Cryst. Growth Des.* **2005**, *5*, 2197−2209.
(44) Gao, X. Y.; Feng, W. D.; Dai, X. J. Preparation methods of methyl-d_3-amine and salts thereof. WO 2011113369 A1, Sep 22, 2011.
(45) Fulmer, G. R.; Miller, A. J. M.; Sherden, N. H.; Gottlieb, H. E.; Nudelman, A.; Stoltz, B. M.; Bercaw, J. E.; Goldberg, K. I. NMR chemical shifts of trace impurities: common laboratory solvents, organics, and gases in deuterated solvents relevant to the organometallic chemist. *Organometallics* **2010**, *29*, 2176−2179.
(46) Reddy, L. S.; Chandran, S. K.; George, S.; Babu, N. J.; Nangia, A. Crystal Structures ofN-Aryl-N′-4-Nitrophenyl Ureas: Molecular Conformation and Weak Interactions Direct the Strong Hydrogen Bond Synthon. *Cryst. Growth Des.* **2007**, *7*, 2675−2690.
(47) Nyman, J.; Day, G. M. Static and lattice vibrational energy differences between polymorphs. *CrystEngComm* **2015**, *17*, 5154−5165.
(48) Brooks, S. J.; Gale, P. A.; Light, M. E. Anion-binding modes in a macrocyclic amidourea. *Chem. Commun.* **2006**, 4344−4346.
(49) Custelcean, R. Urea-functionalized crystalline capsules for recognition and separation of tetrahedral oxoanions. *Chem. Commun.* **2013**, *49*, 2173−2182.
(50) Amendola, V.; Fabbrizzi, L.; Mosca, L. Anion recognition by hydrogen bonding: urea-based receptors. *Chem. Soc. Rev.* **2010**, *39*, 3889−3915.
(51) Rai, S. K.; Gunnam, A.; Mannava, M. K. C.; Nangia, A. K. Improving the dissolution rate of the anticancer drug dabrafenib. *Cryst. Growth Des.* **2020**, *20*, 1035−1046.

https://dx.doi.org/10.1021/acsomega.0c05908
ACS Omega 2021, 6, 5532−5547